Synaptotagmin 9 modulates spontaneous neurotransmitter release in striatal neurons by regulating substance P secretion

Michael J. Seibert,[1,2] Chantell S. Evans,[3] Kevin S. Stanley,[1] Zhenyong Wu,[1] Joseph S. Briguglio,[1] and Edwin R. Chapman[1]

[1] Howard Hughes Medical Institute and Department of Neuroscience, University of Wisconsin-Madison School of Medicine and Public Health, Madison, WI, 53706.
[2] Neuroscience Training Program
[3] Department of Cell Biology, Duke University School of Medicine

ABSTRACT

Synaptotagmin 9 (SYT9) is a tandem C2-domain Ca^{2+} sensor for exocytosis in neuroendocrine cells; its function in neurons remains unclear. Here, we show that SYT9 does not trigger rapid synaptic vesicle exocytosis in cultured cortical, hippocampal, or striatal neurons; rather, synaptotagmin 1 (SYT1) fulfills this function. SYT9 can regulate evoked synaptic vesicle exocytosis, but only when massively over-expressed. In striatal neurons, loss of SYT9 reduced the rate of spontaneous miniature neurotransmitter release events (minis). To delve into the underlying mechanism, we localized SYT9 in striatal neurons and found that it was targeted to dense core vesicles, where it regulated the release of substance P (SP), a neuropeptide known to modulate mini frequency. Exogenous SP, but not other striatal peptide hormones, completely rescued the *Syt9* KO mini phenotype. Biochemical experiments revealed that Ca^{2+}-binding to the C2A domain of SYT9 serves to regulate membrane fusion *in vitro*, and mutations that disrupt this activity abolished the ability of SYT9 to regulate minis in striatal neurons. We conclude that SYT9 indirectly regulates synaptic transmission in striatal neurons by controlling SP release.

INTRODUCTION

The synaptotagmins (SYTs) are a large family of membrane trafficking proteins: seventeen isoforms have been identified in mammals, each encoded by a distinct gene (Craxton, 2010; Wolfes and Dean, 2020). In addition, most isoforms are thought to undergo alternative splicing, generating further potential diversity within this family (Craxton, 2010). Most isoforms have a single N-terminal transmembrane domain (TMD) with a short intra-luminal domain. In all isoforms, the cytoplasmic domain comprises tandem C2-domains that are connected by a short linker. In at least eight of the seventeen isoforms, the C2-domains serve as Ca^{2+}-dependent anionic lipid-binding motifs (Bhalla et al., 2008; Rickman et al., 2004). Ca^{2+} binding is mediated by acidic side chains in two flexible loops that protrude from each C2-domain (Sutton et al., 1995). In the case of SYT1, Ca^{2+} triggers the penetration of these loops into lipid bilayers and facilitates interactions with SNARE proteins (Chapman, 2008). While membrane penetration is an essential step in Ca^{2+}-triggered exocytosis (Bai et al., 2016; Evans et al., 2015; Liu et al., 2014), the role of SYT-SNARE interactions in membrane fusion remains

unresolved (Bai et al., 2016; Bhalla et al., 2006; Chicka et al., 2008; Das et al., 2020; Van Den Bogaart et al., 2011; Zhou et al., 2017).

A current goal is to understand the functional diversity among all members of the SYT family of proteins. SYT1 and SYT2 have been heavily studied and are multifunctional proteins that serve as Ca^{2+} sensors that trigger rapid, synchronous synaptic vesicle (SV) exocytosis in neurons (Geppert et al., 1994; Pang et al., 2006a; Stevens and Sullivan, 2003). SYT1 has also been shown to regulate SV docking (Chang et al., 2018; Liu et al., 2009; Reist et al., 1998), endocytosis (Jorgensen et al., 1995; Nicholson-Tomishima and Ryan, 2004; Poskanzer et al., 2003; Yao et al., 2012), and spontaneous release (Bai et al., 2016; Courtney et al., 2019; DiAntonio and Schwarz, 1994; Kerr et al., 2008; Littleton et al., 1994; Vevea and Chapman, 2020). Importantly, SYT1 and SYT2 form a closely related clade with one more family member, SYT9 (Rickman et al., 2004); this homology prompted the idea that SYT9 also functions as a fast Ca^{2+} sensor for SV release (Xu et al., 2007). For clarity, we note that SYT9 is sometimes referred to as SYT5, and vice versa; the SYT9 studied here has 386 residues (NCBI Gene accession # 53420) whereas SYT5 has 491 residues (NCBI Gene accession #60510).

Along with SYT1, SYT9 co-regulates catecholamine secretion from dense core vesicles (DCV) in PC12 cells (Fukuda et al., 2002; Lynch and Martin, 2007), and was shown to regulate the release of follicle-stimulating hormone (FSH) from DCVs in the gonadotrophs of female, but not male, mice (Roper et al., 2015). However, although SYT9 is widely expressed in the brain [(Mittelsteadt et al., 2009) note: SYT9 is referenced in this study as SYT5], its function in neurons remains controversial. As alluded to above, one report concluded that SYT9 serves as a Ca^{2+} sensor for rapid SV exocytosis in cultured striatal neurons (Xu et al., 2007). In contrast, SYT9 failed to support SV exocytosis in *Syt1* KO hippocampal neurons, and pHluorin-tagged SYT9 underwent regulated exocytosis in both axons and dendrites of hippocampal neurons, with kinetics suggestive of DCV fusion (Dean et al., 2012a).

To address and clarify the function of SYT9, we studied synaptic transmission in cultured hippocampal, cortical, and striatal neurons obtained from *Syt9* KO mice and *Syt1* cKO mice. We show that all three classes of neurons express both SYT9 and SYT1, but loss of SYT9 had no discernable effect on evoked neurotransmitter release, while loss of SYT1 disrupted rapid transmission in all three neuronal preparations. SYT9 was able to rescue the loss of synchronous release that is characteristic of *Syt1* KO neurons, but only when over-expressed by ~25-fold, which matched the expression levels of endogenous SYT1. Interestingly, loss of SYT9 in cultured striatal neurons resulted in a specific and unexpected phenotype: a decrease in the spontaneous miniature (mini) SV fusion rate. We then discovered that SYT9 was co-localized with substance P (SP), a DCV peptide hormone known to be enriched in striatal neurons. Moreover, loss of SYT9 impaired action potential-triggered release of SP. Importantly, supplementing the bath with this neuropeptide rescued the mini phenotype. These findings reveal a mechanism in which SYT9 indirectly regulates spontaneous transmission in striatal neurons by directly regulating secretion of the neuromodulator, substance P.

RESULTS

Synaptotagmin-9 is not required for fast, synchronous neurotransmitter release in cultured neurons

Immunoblot analysis of neuronal culture lysates revealed that synaptotagmin 1 (SYT1) and synaptotagmin 9 (SYT9) are expressed in cortical (CTX), hippocampal (HIP), and striatal neurons (STR) (**Fig. 1a,e**). By including known amounts of purified recombinant SYT1 cytoplasmic domain (C2AB) or SYT9 (full-length) as standards on these blots we were able to determine the absolute expression levels via quantitative densitometry (**Fig. 1b,f**). This analysis revealed that SYT1 and SYT9 were ~0.1% and ~0.004% of the total protein in each of the neuronal lysates, respectively. Hence, SYT1 expression is ~25 times greater than SYT9 in all three classes of neurons.

A prior study suggested that SYT1 and SYT9 serve as partially redundant Ca^{2+} sensors in striatal neurons and that SYT9 can fully rescue fast release in *Syt1* KO cortical neurons (Xu et al., 2007). However, this is difficult to reconcile with the established finding that loss of SYT1 in hippocampal and cortical neurons disrupts virtually all synchronous release (Geppert et al., 1994; Maximov and Südhof, 2005). If SYT9 is a sensor for synchronous release, some fast release should persist in the *Syt1* KO neurons. To address this conundrum, whole-cell patch-clamp experiments were carried out using cultured neurons from *Syt1* cKO and *Syt9* KO mice. In striatal neurons, ablation of SYT1 expression eliminated fast, synchronous neurotransmitter release with an 8-fold reduction in evoked inhibitory postsynaptic current (eIPSC) amplitude (**Fig. 1c,d**). Disruption of SYT9 expression, however, did not result in any change in eIPSC amplitude or kinetics in striatal neurons (**Fig. 1g,h; S1**). Results were analogous in cultured cortical and hippocampal neurons (**Supp. Fig. 1**). Evoked release during a stimulus train was also unaffected in *Syt9* KO cortical, hippocampal, and striatal neurons, further demonstrating that this isoform does not impact evoked transmission (**Supp. Fig. 2**). We conclude that endogenous SYT9 is unable to support synchronous release in absence of SYT1, perhaps because of the relatively low expression level of this protein.

SYT9 rescues SYT1 KO phenotypes only when over-expressed

Xu et al. (2007) reported that SYT9 over-expression can functionally rescue synchronous neurotransmitter release in cultured *Syt1* KO cortical neurons(Xu et al., 2007). Similar findings were made with overexpression of SYT9 in the calyx of Held slice preparation lacking its primary Ca^{2+} sensor, SYT2 (Kochubey et al., 2016). Given the observation that endogenous SYT9 is expressed at levels ~25-fold lower than SYT1 (**Fig. 1b,f**), a quantitative approach was taken to re-evaluate this previously reported rescue activity. Cultured *Syt1* cKO cortical neurons were treated at DIV1 with a CRE lentivirus to disrupt SYT1 expression and then transduced at DIV5 with lentivirus to express SYT9 with an N-terminal pHluorin tag (pH-SYT9). The pH-SYT9 lentivirus was titered such that expression of pH-SYT9 in the + CRE neurons would be either 1x or 25x the endogenous SYT9 expression level; the latter condition matching the levels of endogenous SYT1 (**Fig. 2a**; **Fig. 1**). Ablation of SYT1 expression again resulted in a loss of fast, synchronous neurotransmission, and 1x over-expression of pH-SYT9 had no effect on eIPSC amplitude but partially rescued the eIPSC rise kinetics (**Fig.2b-d**). However, 25x over-expression of pH-SYT9 significantly rescued the eIPSC amplitude (60% compared to -CRE) and completely rescued the eIPSC time-to-peak (**Fig. 2b-d**). The 25x over-expression condition also rescued the decay time of the + CRE condition (**Supp. Fig. 3**) So, only upon robust over-expression can SYT9 rescue evoked responses in neurons lacking SYT1 (Kochubey et al., 2016; Xu et al., 2007).

SYT1 is a multifunctional protein that also serves to clamp spontaneous neurotransmitter release under resting conditions (Bai et al., 2016; Chicka et al., 2008; Courtney et al., 2019; Liu et al., 2014; Vevea and Chapman, 2020). To investigate whether over-expressed pH-SYT9 can clamp spontaneous fusion, miniature inhibitory postsynaptic currents (mIPSCs, also called minis) were recorded in the presence of tetrodotoxin, to block action potentials (**Fig. 2e**). Disruption of SYT1 resulted in a ~3-fold increase in mIPSC frequency, with no rescue observed in the 1x pH-SYT9 over-expression condition. In contrast, 25x over-expression of SYT9 resulted in a complete rescue of clamping activity (**Fig. 2f**). mIPSC amplitude and rise and decay kinetics were unaffected across conditions (**Fig. 2g**). Taken together, these findings indicate that SYT9 can rescue evoked release and clamp spontaneous release, in *Syt1* cKO neurons, when it is massively over-expressed.

To investigate how the localization of over-expressed SYT9 may function to support SV release, we utilized the N-terminal pHluorin tag to differentiate between pools in the plasma membrane versus internal compartments (see methods and Courtney et al., 2019). We co-stained with antibodies against synaptophysin (SYP), to label SVs. The internal fraction in the 1x over-expression condition showed some degree of colocalization with SYP, and the internal fraction of 25x pH-SYT9 had a higher degree of colocalization. For comparison, we note that endogenous SYT9 colocalized with SYP to a similar degree as 1x over-expression, while 25x over-expression colocalized with SYP to a similar degree as endogenous SYT1 (**Fig. 2h, i)**. These results are congruent with the idea that some SYT9 may be present on SVs, as indicated in proteomic studies (Takamori et al., 2006; Taoufiq et al., 2020). However, these levels are too low to support evoked release or to clamp spontaneous release, at least in the types of neurons under study here.

Decreased mIPSC frequency in SYT9 KO striatal neurons

To further characterize neurotransmission in *Syt9* KO mice, spontaneous release from cultured striatal neurons was measured and compared to WT controls. We reiterate that all aspects of release evoked by single action potentials were normal (**Fig. 1g**); however, the mIPSC frequency in *Syt9* KO striatal neurons was reduced 2-fold (**Fig. 3a,c**), with no effect on the amplitude or kinetics of these spontaneous quantal events (**Fig. 3b**). Re-expression of SYT9 was sufficient to rescue the decreased mIPSC frequency (**Fig. 3c**). Interestingly, when the same experiment was performed using cortical and hippocampal neurons, loss of SYT9 did not affect spontaneous release rates (**Supp. Fig. 4**), suggesting that this phenotype was specific for striatal neurons, most of which are GABAergic medium spiny neurons (MSNs) (Kemp and Powell, 1971). Importantly, the density of synapses was unchanged between WT and *Syt9* KO striatal neurons (**Supp. Fig. 5**).

We note that most mIPSCs are Ca^{2+}-dependent and are thought to use the same Ca^{2+} sensors as evoked synchronous and asynchronous release, including SYT1 and Doc2 (Courtney et al., 2018; Groffen et al., 2010; Xu et al., 2009). The insufficiency of endogenous SYT9 to drive evoked release argues against the idea that it is a Ca^{2+} sensor for mIPSCs. Furthermore, the specificity of the mIPSC phenotype for striatal versus hippocampal or cortical neurons suggests a cell-specific mechanism for the action of SYT9 in spontaneous release. SYT9 is targeted to DCVs in a variety of tissues (Fukuda et al., 2002; Iezzi et al., 2005; Lynch and Martin, 2007; Roper et al., 2015), and some DCV neuropeptides have been shown to

regulate aspects of synaptic transmission (Cao et al., 2011; Dean et al., 2009; He et al., 2019). This prompts the idea that SYT9 might regulate minis indirectly, potentially by controlling the release of neuromodulators.

SYT9 regulates the secretion of substance P-pHluorin from striatal neurons

To investigate the mechanism by which SYT9 regulates mIPSC frequency, we conducted further localization studies. Since the *Syt9* KO phenotype was specific for striatal neurons, we focused on investigating striatum-specific DCV neuropeptides. Among these, substance P (SP) was of particular interest because it has been shown to regulate mIPSC frequency in striatal neurons through its action on the neurokinin 1 receptor (NK1R) (He et al., 2019). Interestingly, SP is not enriched in hippocampal or cortical neurons (Shults et al., 1984), where the mIPSC phenotype was not observed.

Specific antibodies for SP are not available, so we transduced striatal neurons with a lentivirus that expresses an SP-pHluorin (SP-pH) fusion protein and performed immunocytochemistry (ICC) to assess co-localization of the pHluorin tag with endogenous SYT9. Strikingly, SYT9 was colocalized with SP-pH (**Fig. 4a,b**). The correct localization of the SP-pH construct was confirmed by staining for chromogranin B (CHGB), a canonical DCV marker in neurons (**Fig. 4c,d**). In summary, these findings demonstrate the presence of SYT9 on DCVs that bear a neuropeptide known to regulate mIPSC frequency (He et al., 2019)

Next, we sought to determine whether SYT9 regulates SP release from DCVs in striatal neurons. To optically measure SP secretion events at single-event resolution, WT and *Syt9* KO neurons were sparsely transfected with a plasmid encoding SP-pH. SP-pH fluorescence is quenched in the low pH environment of the DCV lumen; upon exocytosis, the pHluorin is rapidly dequenched, yielding a large increase in fluorescence intensity (**Fig 4e**). In cultured neurons, repetitive high-frequency electrical stimulation (i.e.,16 bursts of 50 APs at 50Hz) has been shown to effectively trigger these release events (Persoon et al., 2018); this paradigm was used in our experiments and yielded robust exocytosis (**Fig. 4f**). DCV fusion was quantified in WT and *Syt9* KO striatal neurons, where the released fraction was calculated as the number of fusion events divided by the total number of SP-pH vesicles in a single neuron. The total SP-pH DCV pool was estimated by perfusing neurons with NH_4Cl to alkalinize the lumen of DCVs and dequench the pHluorin reporter; no significant differences were observed between the WT and KO (**Fig 4g**). In WT neurons the released fraction was ~10%. In *Syt9* KO neurons this was reduced by ~61% (**Fig. 4h, i**), with only ~3.9% of the vesicles being released. Fusion event duration was also measured in WT and *Syt9* KO neurons; there appeared to be a small population of long-duration release events that was absent in the WT (**Fig. 4j**), hinting at a potential role of SYT9 in regulating the fate of fusion pores, as shown for other SYT isoforms (Wolfes and Dean, 2020). Finally, loss of SYT9 had no apparent effect on the transport of SP-pH vesicles, suggesting that the observed reductions in SP secretion were not secondary to trafficking defects (**Supp. Fig. 6**).

Application of exogenous substance P rescues SYT9 KO mIPSC phenotype

Since SYT9 regulates SP release (**Fig. 4**), and SP is known to modulate mIPSC frequency in striatal neurons (He et al., 2019), we sought to determine whether the *Syt9* KO phenotype could be rescued via acute application of the exogenous neuropeptide. In addition to

SP, enkephalins, dynorphins, and cholecystokinin are also enriched in the striatum (Angulo and McEwen, 1994; Krause et al., 1987), so we also assayed the effects of each of these neuropeptides (**Fig. 5a**). Acute addition of SP to the bath fully rescued the decreased mIPSC frequency *in Syt9* KO neurons. Rescue was also observed using GR73632, a synthetic NK1R agonist. In contrast, dynorphin A (DynA), Leu-enkephalin (L-Enk), and cholecystokinin (CCK8) (**Fig. 5b**) had no effect. Also, we found that SP supplementation did not significantly change the mIPSC frequency of WT neurons. Finally, application of SR140333, a synthetic NK1R antagonist (Jung et al., 1994), to WT neurons fully phenocopied the *Syt9* KO; mIPSC frequency was reduced ~2-fold (**Fig. 5b**). No differences in mIPSC amplitude were observed across all conditions (**Fig. 5c**)**.** In summary, SYT9 regulates SP release, and activation of the NK1R is pivotal in the regulation of mIPSCs in striatal neurons.

SP presumably modulates spontaneous release rates in striatal neurons by binding the NK1 receptor and activating G_q, resulting in the generation of IP_3 and the mobilization of Ca^{2+} from internal stores. While basal presynaptic $[Ca^{2+}]_i$ did not appear to be altered in the *Syt9* KO striatal neurons (**Supp. Fig. 7**), local, transient increases in $[Ca^{2+}]_i$ mediated by IP_3 receptors from presynaptic ER, drive spontaneous neurotransmitter release in pyramidal neurons (Emptage et al., 2001; Simkus and Stricker, 2002), and may belie the decreased mIPSC phenotype observed in our studies.

Ca^{2+}-binding to the C2A domain of SYT9 is crucial for its function *in vitro* and in neurons

The findings presented thus far suggest a model in which SYT9 regulates membrane fusion by acting as a Ca^{2+} sensor that regulates SP release which, in turn, modulates mini frequency. To further test this model, we sought to identify structural elements in SYT9 that serve to directly regulate membrane fusion *in vitro*, and then correlate these findings with the function of SYT9 in regulating mini frequency. For these experiments, we used soluble, cytoplasmic fragments of SYT9, and for comparison, SYT1, in a 'split t-SNARE' *in vitro* fusion assay (Bhalla et al., 2006) that mimics fusion of synaptic vesicles with the plasma membrane in cells. In this assay, SYT fragments must first fold SNAP-25B onto membrane-embedded syntaxin 1A (SYX1A) for fusion with synaptobrevin 2 (SYB2)-bearing liposomes to occur. Consistent with a previous study (Roper et al., 2015), the cytoplasmic domains of both SYT1 and SYT9 stimulated fusion to similar extents in the presence of Ca^{2+} (omitted for clarity in **Fig. 6a** left panel, but quantified in **Fig. 6a**-right panel). We extended these experiments by testing the isolated C2-domains of each isoform and found that the C2A domain of SYT9 strongly stimulated fusion in response to Ca^{2+}, while C2B had little effect (**Fig. 6**-left and right panels). This is in sharp contrast to SYT1, where C2B, but not C2A, facilitated fusion (**Fig. 6**-left and right panels)(Gaffaney et al., 2008). Additionally, we utilized Ca^{2+} ligand mutants (CLMs), in which two native Asp residues that serve as conserved Ca^{2+} ligands in numerous isoforms were substituted with Asn, in either C2A or C2B of SYT9. These mutations disrupted the Ca^{2+} binding activity (shown further below) of each C2-domain and abolished the ability of the C2A domain of SYT9 to stimulate membrane fusion in response to Ca^{2+} (**Fig. 6b**). Hence, these two related isoforms have diverged unexpectedly, with C2A serving as the primary Ca^{2+} sensing domain in SYT9, while C2B is more crucial in SYT1.

Since SYT1 regulates fusion via interactions with membranes that harbor anionic phospholipids (Bai et al., 2016; Bhalla et al., 2005; Liu et al., 2014), we assayed the ability of

SYT9 to bind phosphatidylserine (PS)-harboring membranes in the presence and absence of Ca^{2+}. A previous study reported that C2A, but not C2B, bound to PS-bearing vesicles (Shin et al., 2004). We found that each of the isolated C2-domains efficiently bound to liposomes, in response to Ca^{2+}, when the mole fraction of PS was increased from 15% to 25%; this interaction is physiologically relevant since PS is ~22% of the inner leaflet of the plasma membrane (Hamilton et al., 2000) (**Fig. 6b**).

We also directly measured Ca^{2+} binding to the isolated C2-domains of SYT9, using isothermal titration calorimetry (ITC); calorimetry data for SYT1 has been previously reported (Evans et al., 2016; Radhakrishnan et al., 2009). Ca^{2+} binding to SYT9 C2A was endothermic and binding to C2B was exothermic (**Fig. 6c**). When fitted with a sequential binding site model, C2A exhibited three binding sites with K_d values of 53 µM, 182 µM, and 337 µM; C2B had two binding sites, with K_d values of 43 µM and 500 µM (see **Supplementary Table 1** for all thermodynamic values). Interestingly, the K_d value for the third binding site of C2A (337 µM) was significantly lower than the value reported for SYT1 (K_d > 1 mM (Evans et al., 2016; Radhakrishnan et al., 2009; Ubach et al., 1998). Titrations were also performed on the CLM forms of isolated C2A or C2B, described above, and these constructs yielded little to no signal, confirming they fail to bind Ca^{2+} (**Fig. 6c**).

Finally, if our model is correct, the biochemical results above suggest that Ca^{2+} binding to C2A, but not C2B, should disrupt the ability of SYT9 to promote minis. We, therefore, conducted patch-clamp recordings of *Syt9* KO striatal neurons that expressed each full-length CLM construct. Again, complete rescue of mIPSC frequency was observed using WT SYT9. In sharp contrast, SYT9 $C2A_mB_m$, which cannot bind Ca^{2+} via either C2-domain, failed to rescue the mini phenotype. Consistent with our model, $C2A_mB$ also failed to rescue (**Fig. 7a**), while $C2AB_m$ was as effective as the WT protein (**Fig. 7b**; note: no changes in mini amplitude were observed across conditions (**Fig. 7c**)). In summary, Ca^{2+} binding to the C2A domain, but not the C2B domain, underlies the ability of SYT9 to regulate membrane fusion *in vitro* to, in turn, indirectly control the rate of spontaneous release.

DISCUSSION

SYT9 is widely expressed in the brain [(Mittelsteadt et al., 2009) (note: SYT9 is referenced in this study as SYT5)], but KOs lacking this protein have only been characterized using the calyx of Held slice preparation (Kochubey et al., 2016) and cultured striatal neurons (Xu et al., 2007). SYT9 appears to be expressed in the calyx of Held, but loss of this protein did not affect AP-triggered neurotransmitter release (Kochubey et al., 2016). In contrast, in cultured MSNs, Xu et al. (2007) reported a 57% reduction in eIPSC amplitude in *Syt9* KO striatal neurons. However, this finding has not been reproduced, and it is difficult to reconcile with the expression patterns of SYT9 and SYT1. Namely, SYT9 is expressed at similar levels in cortical, hippocampal, and striatal neurons, and it is well established that loss of SYT1 abolishes synchronous release in both cortical and hippocampal neurons (Geppert et al., 1994; Maximov and Südhof, 2005) (**Fig 1**). So, it is apparent that endogenous SYT9 does not function as a Ca^{2+} sensor for synchronous SV exocytosis in either of these two classes of neurons (**Fig. 1; Supp. Fig. 1**). Here, we extended these observations to cultured striatal neurons and found that SYT1, but not endogenous SYT9, drives rapid SV exocytosis. We went on to show that SYT9 is largely

localized to SP-bearing DCVs in striatal neurons, where it regulates the release of this neuropeptide to indirectly control mIPSC frequency. Evidently, at least some isoforms of SYT have become specialized to control the release of neuropeptides that impact synaptic function (Cao et al., 2011; Dean et al., 2012b, 2009; Roper et al., 2015). As discussed under Results, it is tempting to speculate the divergence of numerous SYT isoforms might enable the differential release of myriad distinct neuromodulators and hormones, in response to different patterns of activity.

We found that SYT9 is expressed at ~25-fold lower levels than SYT1 (**Fig. 1**). Given the estimate of ~15 copies of SYT1 per SV (Takamori et al., 2006), the abundance of SYT9 on SVs would, on average, be expected to be low, particularly since its primary localization appears to be on DCVs. Some fraction of SYT9 does colocalize with canonical SV markers (**Fig. 2**; Xu et al., 2007), and SYT9 was detected in proteomic studies of purified SVs (Takamori et al., 2006; Taoufiq et al., 2020) (note: again, in these studies, SYT9 was referred to as SYT5). Thus, it remains possible that there could be limited populations of SVs, in discrete brain regions, that harbor a sufficient copy number of SYT9 molecules to trigger SV exocytosis. However, in our hands, this was not the case in cortical, hippocampal, or striatal neurons (**Supp. Fig. 1**). It should also be emphasized that DCVs are often present in presynaptic nerve terminals (Persoon et al., 2018; Radhakrishnan et al., 2021), and hence can contribute to the degree of co-localization of SYT9 with SV markers, likely causing overestimation of the occurrence of SYT9 on SVs.

While our experiments suggest that SYT9 may be a Ca^{2+} sensor for SP release from striatal neurons, some degree of regulated release persisted in the KO (**Fig. 4**), suggesting that additional Ca^{2+} sensors may be present on SP-bearing DCVs. Indeed, SYT1 was present on SP-bearing DCVs purified from rabbit optic nerve (Berg et al., 2000). Additionally, in hippocampal neurons, SYT1 and SYT7 have both been implicated in DCV exocytosis (van Westen et al., 2021), suggesting multiple roles for these Ca^{2+} sensors. We also note that SYT4 regulates the release of brain-derived neurotrophic factor (BDNF) (Dean et al., 2009), and SYT10 regulates the secretion of IGF-1 from DCVs in neurons (Cao et al., 2011). Collectively, these findings, combined with the observations in the current study, support the idea that the SYTs have diverged, at least in part, to control different forms of DCV exocytosis (Dean et al., 2012a). We also reiterate that the *Syt9* KO mIPSC phenotype appears to be specific for striatal neurons, which robustly express SP. The function of SYT9 in cortical and hippocampal neurons remains unknown. We speculate that it regulates the release of neuropeptides; a future goal is to address this issue via co-localization studies and by isolating and characterizing SYT9-bearing organelles from these cells.

Further, regarding the diversity of SYT isoforms, our finding that the C2A domain of SYT9 serves as the crucial Ca^{2+}-sensing motif for fusion was unexpected. SYT9 forms a clade with SYT1/2, and Ca^{2+} ligand mutations in the C2B-domain of SYT1 clearly disrupt function (Nishiki and Augustine, 2004), while similar mutations in C2A have been reported to either have no effect (Fernández-Chacón et al., 2002), to be gain-of-function (Pang et al., 2006b; Stevens and Sullivan, 2003), or to cause partial loss-of-function (Shin et al., 2009). Moreover, the isolated C2B domain of SYT1, but not the C2A domain, regulates fusion *in vitro* (**Fig. 6**; Gaffaney et al., 2008). In the case of SYT9, we found that Ca^{2+}-binding to the C2A domain, but not the C2B domain, was required to stimulate fusion *in vitro* (**Fig. 6**). Apparently, this shuffling

of C2-domain function is tolerated, as SYT9 can rescue evoked neurotransmitter release and in *Syt1* cKO neurons, when sufficiently over-expressed (**Fig. 2**).

Returning to the physiology, we emphasize that the striatum is a specialized structure with a dense local network largely composed of MSNs and their axon collaterals; while a substantial fraction of these neurons project to other brain regions, direct synaptic communication between MSNs also occurs (Koos et al., 2004; Tunstall et al., 2002); this is the condition recapitulated in our experiments using cultured striatal neurons. Subpopulations of MSNs release substance P within the striatum (Gerfen, 1992) and also harbor NK1 receptors (Almeida et al., 2004). We observed modulation of MSN-MSN transmission by SP in culture, and the next step will be to measure such modulation in acute slice preparations of the striatum. In addition, MSNs project to targets in the substantia nigra and globus pallidus, and recordings from brain slices that encompass the striatum along with these other structures will address the role of SYT9-regulated SP release at terminals that innervate these target cells. Indeed, it has been shown that SP released from MSNs discretely enhances center-surround contrast of striosomal dopamine signals, by modulating dopamine release from neurons that project from the substantial nigra onto striatal targets (Brimblecombe and Cragg, 2015). Hence, slice recordings are an important future direction of this work.

In summary, we suggest that SP modulates spontaneous release rates by binding the NK1 receptor and activating G_q, resulting in the generation of IP_3 and the mobilization of Ca^{2+} from internal stores (**Fig. 8**), thus increasing mini frequency. Indeed, localized increases in $[Ca^{2+}]_I$, mediated by IP_3 receptors in the presynaptic ER have been reported to drive spontaneous release in pyramidal neurons (Emptage et al., 2001; Simkus and Stricker, 2002). So, a future goal is to compare these brief Ca^{2+} transients, akin to Ca^{2+} sparks in muscle cells, in WT and *Syt9* KO striatal neurons. Finally, we emphasize that the highest expression levels of SYT9 in mouse brain occur in the pituitary gland and hypothalamus, which are particularly rich sources of numerous classes of DCVs (Roper et al., 2015). It will be interesting to investigate whether SYT9 regulates the release of hypothalamic hormones.

REFERENCES

Almeida TA, Rojo J, Nieto PM, Pinto FM, Hernandez M, Martín JD, Candenas ML. 2004. Tachykinins and Tachykinin Receptors: Structure and Activity Relationships. *Curr Med Chem* **11**:2045–2081. doi:10.2174/0929867043364748

Angulo JA, McEwen BS. 1994. Molecular aspects of neuropeptide regulation and function in the corpus striatum and nucleus accumbens. *Brain Res Rev* **19**:1–28. doi:10.1016/0165-0173(94)90002-7

Bai H, Xue R, Bao H, Zhang L, Yethiraj A, Cui Q, Chapman ER. 2016. Different states of synaptotagmin regulate evoked versus spontaneous release. *Nat Commun* **7**:1–9. doi:10.1038/ncomms10971

Berg EA, Johnson RJ, Leeman SE, Boyd N, Kimerer L, Fine RE. 2000. Isolation and characterization of substance P-containing dense core vesicles from rabbit optic nerve and termini. *J Neurosci Res* **62**:830–839. doi:10.1002/1097-4547(20001215)62:6<830::AID-JNR10>3.0.CO;2-E

Bhalla A, Chicka MC, Chapman ER. 2008. Analysis of the synaptotagmin family during

reconstituted membrane fusion: Uncovering a class of inhibitory isoforms. *J Biol Chem* **283**:21799–21807. doi:10.1074/jbc.M709628200

Bhalla A, Chicka MC, Tucker WC, Chapman ER. 2006. Ca2+-synaptotagmin directly regulates t-SNARE function during reconstituted membrane fusion. *Nat Struct Mol Biol* **13**:323–330. doi:10.1038/nsmb1076

Bhalla A, Tucker WC, Chapman ER. 2005. Synaptotagmin Isoforms Couple Distinct Ranges of Ca2+, Ba2+, and Sr2+ Concentration to SNARE-mediated Membrane Fusion. *Mol Biol Cell* **16**:4755–4764. doi:10.1091/mbc.E05-04-0277

Bradberry MM, Chapman ER. 2022. All-optical monitoring of excitation–secretion coupling demonstrates that SV2A functions downstream of evoked Ca2+ entry. *J Physiol* **600**:645–654. doi:10.1113/JP282601

Brimblecombe KR, Cragg SJ. 2015. Substance P weights striatal dopamine transmission differently within the striosome-matrix axis. *J Neurosci* **35**:9017–9023. doi:10.1523/JNEUROSCI.0870-15.2015

Cao P, Maximov A, Südhof TC. 2011. Activity-dependent IGF-1 exocytosis is controlled by the Ca 2+-sensor synaptotagmin-10. *Cell* **145**:300–311. doi:10.1016/j.cell.2011.03.034

Chang S, Trimbuch T, Rosenmund C. 2018. Synaptotagmin-1 drives synchronous Ca2+ -triggered fusion by C2B-domain-mediated synaptic-vesicle-membrane attachment. *Nat Neurosci* **21**:33–42. doi:10.1038/s41593-017-0037-5

Chapman ER. 2008. How does synaptotagmin trigger neurotransmitter release? *Annu Rev Biochem*. doi:10.1146/annurev.biochem.77.062005.101135

Chicka MC, Hui E, Liu H, Chapman ER. 2008. Synaptotagmin arrests the SNARE complex before triggering fast, efficient membrane fusion in response to Ca2+. *Nat Struct Mol Biol* **15**:827–835. doi:10.1038/nsmb.1463

Courtney NA, Bao H, Briguglio JS, Chapman ER. 2019. Synaptotagmin 1 clamps synaptic vesicle fusion in mammalian neurons independent of complexin. *Nat Commun* **10**. doi:10.1038/s41467-019-12015-w

Courtney NA, Briguglio JS, Bradberry MM, Greer C, Chapman ER. 2018. Excitatory and Inhibitory Neurons Utilize Different Ca2+ Sensors and Sources to Regulate Spontaneous Release. *Neuron* **98**:977-991.e5. doi:10.1016/j.neuron.2018.04.022

Craxton M. 2010. A manual collection of Syt, Esyt, Rph3a, Rph3al, Doc2, and Dblc2 genes from 46 metazoan genomes - an open access resource for neuroscience and evolutionary biology. *BMC Genomics* **11**. doi:10.1186/1471-2164-11-37

Das D, Bao H, Courtney KC, Wu L, Chapman ER. 2020. Resolving kinetic intermediates during the regulated assembly and disassembly of fusion pores. *Nat Commun* **11**:231. doi:10.1038/s41467-019-14072-7

Dean C, Dunning FM, Liu H, Bomba-Warczak E, Martens H, Bharat V, Ahmed S, Chapman ER. 2012a. Axonal and dendritic synaptotagmin isoforms revealed by a pHluorin-syt functional screen. *Mol Biol Cell* **23**:1715–1727. doi:10.1091/mbc.e11-08-0707

Dean C, Liu H, Dunning FM, Chang PY, Jackson MB, Chapman ER. 2009. Synaptotagmin-IV modulates synaptic function and long-term potentiation by regulating BDNF release. *Nat Neurosci* **12**:767–776. doi:10.1038/nn.2315

Dean C, Liu H, Staudt T, Stahlberg MA, Vingill S, Buckers J, Kamin D, Engelhardt J, Jackson MB, Hell SW, Chapman ER. 2012b. Distinct Subsets of Syt-IV/BDNF Vesicles Are Sorted to Axons versus Dendrites and Recruited to Synapses by Activity. *J Neurosci* **32**:5398–5413. doi:10.1523/JNEUROSCI.4515-11.2012

Deo C, Sheu SH, Seo J, Clapham DE, Lavis LD. 2019. Isomeric Tuning Yields Bright and Targetable Red Ca2+ Indicators. *J Am Chem Soc* **141**:13734–13738. doi:10.1021/jacs.9b06092

DiAntonio A, Schwarz TL. 1994. The effect on synaptic physiology of synaptotagmin mutations in drosophila. *Neuron* **12**:909–920. doi:10.1016/0896-6273(94)90342-5

Emptage NJ, Reid CA, Fine A. 2001. Calcium stores in hippocampal synaptic boutons mediate short-term plasticity, store-operated Ca2+entry, and spontaneous transmitter release. *Neuron* **29**:197–208. doi:10.1016/S0896-6273(01)00190-8

Evans CS, He Z, Bai H, Lou X, Jeggle P, Sutton RB, Edwardson JM, Chapman ER. 2016. Functional analysis of the interface between the tandem C2 domains of synaptotagmin-1. *Mol Biol Cell* **27**:979–989. doi:10.1091/mbc.E15-07-0503

Evans CS, Ruhl DA, Chapman ER. 2015. An engineered metal sensor tunes the kinetics of synaptic transmission. *J Neurosci* **35**:11769–11779. doi:10.1523/JNEUROSCI.1694-15.2015

Fernández-Chacón R, Shin OH, Königstorfer A, Matos MF, Meyer AC, Garcia J, Gerber SH, Rizo J, Südhof TC, Rosenmund C. 2002. Structure/function analysis of Ca2+ binding to the C2A domain of synaptotagmin 1. *J Neurosci* **22**:8438–8446. doi:10.1523/jneurosci.22-19-08438.2002

Fukuda M, Kowalchyk JA, Zhang X, Martin TFJ, Mikoshiba K. 2002. Synaptotagmin IX regulates Ca2+-dependent secretion in PC12 cells. *J Biol Chem* **277**:4601–4604. doi:10.1074/jbc.C100588200

Gaffaney JD, Dunning FM, Wang Z, Hui E, Chapman ER. 2008. Synaptotagmin C2B domain regulates Ca2+-triggered fusion in vitro: Critical residues revealed by scanning alanine mutagenesis. *J Biol Chem* **283**:31763–31775. doi:10.1074/JBC.M803355200

Geppert M, Goda Y, Hammer RE, Li C, Rosahl TW, Stevens CF, Südhof TC. 1994. Synaptotagmin I: A major Ca2+sensor for transmitter release at a central synapse. *Cell* **79**:717–727. doi:10.1016/0092-8674(94)90556-8

Gerfen CR. 1992. The neostriatal mosaic: multiple levels of compartmental organization. *Trends Neurosci*. doi:10.1016/0166-2236(92)90355-C

Groffen AJ, Martens S, Arazola RD, Cornelisse LN, Lozovaya N, De Jong APH, Goriounova NA, Habets RLP, Takai Y, Borst JG, Brose N, McMahon HT, Verhage M. 2010. Doc2b is a high-affinity Ca2+sensor for spontaneous neurotransmitter release. *Science (80-)* **327**:1614–1618. doi:10.1126/science.1183765

Hamilton J, Greiner R, Salem N. J, Kim HY. 2000. n-3 fatty acid deficiency decreases phosphatidylserine accumulation selectively in neuronal tissues. *Lipids* **35**:863–869. doi:10.1007/S11745-000-0595-x

He Z-X, Liu T-Y, Yin Y-Y, Song H-F, Zhu X-J. 2019. Substance P plays a critical role in synaptic transmission in striatal neurons. *Biochem Biophys Res Commun* **511**:369–373. doi:S0006291X19302438

Hudson AW, Birnbaum MJ. 1995. Identification of a nonneuronal isoform of synaptotagmin. *Proc Natl Acad Sci* **92**:5895–5899. doi:10.1073/pnas.92.13.5895

Iezzi M, Eliasson L, Fukuda M, Wollheim CB. 2005. Adenovirus-mediated silencing of Synaptotagmin 9 inhibits Ca 2+-dependent insulin secretion in islets. *FEBS Lett* **579**:5241–5246. doi:10.1016/j.febslet.2005.08.047

Jorgensen EM, Hartweig E, Schuske K, Nonet ML, Jin Y, Horvitz HR. 1995. Defective recycling of synaptic vesicles in synaptotagmin mutants of Caenorhabditis elegans. *Nature* **378**:196–199. doi:10.1038/255242a0

Jung M, Calassi R, Maruani J, Barnouin M, Souilhac J, Poncelet M, Gueudet C, Emondsalt X, Soubrié B, Brelière J, Le Fur G. 1994. Neuropharmacological characterization of SR 140333, a non peptide antagonist of NK1 receptors. *Neuropharmacology* **33**:167–179.

Kemp JM, Powell TP. 1971. The structure of the caudate nucleus of the cat: light and electron microscopy. *Philos Trans R Soc Lond B Biol Sci* **262**:383–401. doi:10.1098/rstb.1971.0102

Kerr AM, Reisinger E, Jonas P. 2008. Differential dependence of phasic transmitter release on synaptotagmin 1 at GABAergic and glutamatergic hippocampal synapses. *Proc Natl Acad Sci U S A* **105**:15581–15586. doi:10.1073/pnas.0800621105

Kim SH, Ryan TA. 2009. Synaptic vesicle recycling at CNS synapses without AP-2. *J Neurosci* **29**:3865–3874. doi:10.1523/JNEUROSCI.5639-08.2009

Kochubey O, Babai N, Schneggenburger R. 2016. A Synaptotagmin Isoform Switch during the Development of an Identified CNS Synapse. *Neuron* **90**:984–999. doi:10.1016/j.neuron.2016.04.038

Koos T, Tepper JM, Wilson CJ. 2004. Comparison of IPSCs evoked by spiny and fast-spiking neurons in the neostriatum. *J Neurosci* **24**:7916–7922. doi:10.1523/JNEUROSCI.2163-04.2004

Krause JE, Chirgwin JM, Carter MS, Xu ZS, Hershey AD. 1987. Three rat preprotachykinin mRNAs encode the neuropeptides substance P and neurokinin A. *Proc Natl Acad Sci U S A* **84**:881–885. doi:10.1073/pnas.84.3.881

Kügler S, Kilic E, Bähr M. 2003. Human synapsin 1 gene promoter confers highly neuron-specific long-term transgene expression from an adenoviral vector in the adult rat brain depending on the transduced area. *Gene Ther*. doi:10.1038/sj.gt.3301905

Ladner CL, Yang J, Turner RJ, Edwards RA. 2004. Visible fluorescent detection of proteins in polyacrylamide gels without staining. *Anal Biochem* **326**:13–20. doi:10.1016/j.ab.2003.10.047

Littleton JT, Stern M, Perin M, Bellen HJ. 1994. Calcium dependence of neurotransmitter release and rate of spontaneous vesicle fusions are altered in Drosophila synaptotagmin mutants. *Proc Natl Acad Sci U S A* **91**:10888–10892. doi:10.1073/pnas.91.23.10888

Liu H, Bai H, Xue R, Takahashi H, Edwardson JM, Chapman ER. 2014. Linker mutations reveal the complexity of synaptotagmin 1 action during synaptic transmission. *Nat Neurosci* **17**:670–677. doi:10.1038/nn.3681

Liu H, Dean C, Arthur CP, Dong M, Chapman ER. 2009. Autapses and networks of hippocampal neurons exhibit distinct synaptic transmission phenotypes in the absence of synaptotagmin I. *J Neurosci* **29**:7395–7403. doi:10.1523/JNEUROSCI.1341-09.2009

Lois C, Hong EJ, Pease S, Brown EJ, Baltimore D. 2002. Germline transmission and tissue-specific expression of transgenes delivered by lentiviral vectors. *Science (80-)* **295**:868–872. doi:10.1126/science.1067081

Lynch KL, Martin TFJ. 2007. Synaptotagmins I and IX function redundantly in regulated exocytosis but not endocytosis in PC12 cells. *J Cell Sci* **120**:617–627. doi:10.1242/jcs.03375

Maximov A, Südhof TC. 2005. Autonomous Function of Synaptotagmin 1 in Triggering Synchronous Release Independent of Asynchronous Release. *Neuron* **48**:547–554. doi:10.1016/J.NEURON.2005.09.006

Miesenböck G, De Angelis DA, Rothman JE. 1998. Visualizing secretion and synaptic transmission with pH-sensitive green fluorescent proteins. *Nature* **394**:192–195.

Mittelsteadt T, Seifert G, Alvárez-Barón E, Steinhäuser C, Becker AJ, Schoch S. 2009. Differential mRNA expression patterns of the synaptotagmin gene family in the rodent brain. *J Comp Neurol*. doi:10.1002/cne.21908

Moro A, Hoogstraaten RI, Persoon CM, Verhage M, Toonen RF. 2021. Quantitative analysis of dense-core vesicle fusion in rodent CNS neurons. *STAR Protoc* **2**:100325. doi:10.1016/j.xpro.2021.100325

Nicholson-Tomishima K, Ryan TA. 2004. Kinetic efficiency of endocytosis at mammalian CNS synapses requires synaptotagmin I. *Proc Natl Acad Sci U S A* **101**:16648–16652. doi:10.1073/pnas.0406968101

Nishiki TI, Augustine GJ. 2004. Dual roles of the C2B domain of synaptotagmin I in synchronizing Ca2+-dependent neurotransmitter release. *J Neurosci* **24**:8542–8550. doi:10.1523/JNEUROSCI.2545-04.2004

Pang ZP, Melicoff E, Padgett D, Liu Y, Teich AF, Dickey BF, Lin W, Adachi R, Südhof TC. 2006a. Synaptotagmin-2 is essential for survival and contributes to Ca 2+ triggering of neurotransmitter release in central and neuromuscular synapses. *J Neurosci* **26**:13493–13504. doi:10.1523/JNEUROSCI.3519-06.2006

Pang ZP, Shin OH, Meyer AC, Rosenmund C, Südhof TC. 2006b. A gain-of-function mutation in synaptotagmin-1 reveals a critical role of Ca2+-dependent soluble N-ethylmaleimide-sensitive factor attachment protein receptor complex binding in synaptic exocytosis. *J Neurosci* **26**:12556–12565. doi:10.1523/JNEUROSCI.3804-06.2006

Persoon CM, Moro A, Nassal JP, Farina M, Broeke JH, Arora S, Dominguez N, Weering JR, Toonen RF, Verhage M. 2018. Pool size estimations for dense-core vesicles in mammalian CNS neurons. *EMBO J* **37**. doi:10.15252/embj.201899672

Poskanzer KE, Marek KW, Sweeney ST, Davis GW. 2003. Synaptotagmin I is necessary for compensatory synaptic vesicle endocytosis in vivo. *Nature* **426**:559–563.

Quadros RM, Miura H, Harms DW, Akatsuka H, Sato T, Aida T, Redder R, Richardson GP, Inagaki Y, Sakai D, Buckley SM, Seshacharyulu P, Batra SK, Behlke MA, Zeiner SA, Jacobi AM, Izu Y, Thoreson WB, Urness LD, Mansour SL, Ohtsuka M, Gurumurthy CB. 2017. Easi-CRISPR: A robust method for one-step generation of mice carrying conditional and insertion alleles using long ssDNA donors and CRISPR ribonucleoproteins. *Genome Biol* **18**:1–15. doi:10.1186/s13059-017-1220-4

Radhakrishnan A, Li X, Grushin K, Krishnakumar SS, Liu J, Rothman JE. 2021. Symmetrical arrangement of proteins under release-ready vesicles in presynaptic terminals. *Proc Natl Acad Sci U S A* **118**. doi:10.1073/pnas.2024029118

Radhakrishnan A, Stein A, Jahn R, Fasshauer D. 2009. The Ca2+ affinity of synaptotagmin 1 is markedly increased by a specific interaction of its C2B domain with phosphatidylinositol 4,5-bisphosphate. *J Biol Chem* **284**:25749–25760. doi:10.1074/jbc.M109.042499

Reist NE, Buchanan J, Li J, DiAntonio A, Buxton EM, Schwarz TL. 1998. Morphologically docked synaptic vesicles are reduced in synaptotagmin mutants of Drosophila. *J Neurosci* **18**:7662–7673. doi:10.1523/jneurosci.18-19-07662.1998

Rickman C, Craxton M, Osborne S, Davletov B. 2004. Comparative analysis of tandem C2 domains from the mammalian synaptotagmin family. *Biochem J* **378**:681–686. doi:10.1042/BJ20031407

Roper LK, Briguglio JS, Evans CS, Jackson MB, Chapman ER. 2015. Sex-specific regulation of follicle-stimulating hormone secretion by synaptotagmin 9. *Nat Commun* **6**:1–10. doi:10.1038/ncomms9645

Schindelin J, Arganda-Carreras I, Frise E, Kaynig V, Longair M, Pietzsch T, Preibisch S, Rueden C, Saalfeld S, Schmid B, Tinevez JY, White DJ, Hartenstein V, Eliceiri K, Tomancak P, Cardona A. 2012. Fiji: An open-source platform for biological-image analysis. *Nat Methods* **9**:676–682. doi:10.1038/nmeth.2019

Schmitz SK, Hjorth JJJ, Joemai RMS, Wijntjes R, Eijgenraam S, de Bruijn P, Georgiou C, de Jong APH, van Ooyen A, Verhage M, Cornelisse LN, Toonen RF, Veldkamp W. 2011. Automated analysis of neuronal morphology, synapse number and synaptic recruitment. *J Neurosci Methods* **195**:185–193. doi:10.1016/J.JNEUMETH.2010.12.011

Shin OH, Maximov A, Lim BK, Rizo J, Südhof TC. 2004. Unexpected Ca2+-binding properties of synaptotagmin 9. *Proc Natl Acad Sci U S A* **101**:2554–2559. doi:10.1073/pnas.0308477100

Shin OH, Xu J, Rizo J, Südhof TC. 2009. Differential but convergent functions of Ca2+ binding to synaptotagmin-1 C2 domains mediate neurotransmitter release. *Proc Natl Acad Sci U S A* **106**:16469–16474. doi:10.1073/PNAS.0908798106

Shults CW, Quirion R, Chronwall B, Chase TN, O'Donohue TL. 1984. A comparison of the anatomical distribution of substance P and substance P receptors in the rat central nervous system. *Peptides* **5**:1097–1128. doi:10.1016/0196-9781(84)90177-3

Simkus CRL, Stricker C. 2002. The contribution of intracellular calcium stores to mEPSCs recorded in layer II neurones of rat barrel cortex. *J Physiol* **545**:521–535. doi:10.1113/jphysiol.2002.022103

Stevens CF, Sullivan JM. 2003. The synaptotagmin C2A domain is part of the calcium sensor controlling fast synaptic transmission. *Neuron* **39**:299–308. doi:10.1016/S0896-6273(03)00432-X

Sutton RB, Davletov BA, Berghuis AM, Sudhof TC, Sprang SR. 1995. Structure of the first C2 domain of synaptotagmin I: A novel Ca2+/phospholipid-binding fold. *Cell* **80**:929–938. doi:10.1016/0092-8674(95)90296-1

Takamori S, Holt M, Stenius K, Lemke EA, Grønborg M, Riedel D, Urlaub H, Schenck S, Brügger B, Ringler P, Müller SA, Rammner B, Gräter F, Hub JS, De Groot BL, Mieskes G,

Moriyama Y, Klingauf J, Grubmüller H, Heuser J, Wieland F, Jahn R. 2006. Molecular Anatomy of a Trafficking Organelle. *Cell* **127**:831–846. doi:10.1016/j.cell.2006.10.030

Taoufiq Z, Ninov M, Villar-Briones A, Wang HY, Sasaki T, Roy MC, Beauchain F, Mori Y, Yoshida T, Takamori S, Jahn R, Takahashi T. 2020. Hidden proteome of synaptic vesicles in the mammalian brain. *Proc Natl Acad Sci U S A* **117**:33586–33596. doi:10.1073/PNAS.2011870117

Tunstall MJ, Oorschot DE, Kean A, Wickens JR. 2002. Inhibitory interactions between spiny projection neurons in the rat striatum. *J Neurophysiol* **88**:1263–1269. doi:10.1152/jn.2002.88.3.1263

Ubach J, Zhang X, Shao X, Südhof TC, Rizo J. 1998. Ca2+ binding to synaptotagmin: How many Ca2+ ions bind to the tip of a C2-domain? *EMBO J* **17**:3921–3930. doi:10.1093/emboj/17.14.3921

Van Den Bogaart G, Thutupalli S, Risselada JH, Meyenberg K, Holt M, Riedel D, Diederichsen U, Herminghaus S, Grubmüller H, Jahn R. 2011. Synaptotagmin-1 may be a distance regulator acting upstream of SNARE nucleation. *Nat Struct Mol Biol* **18**:805–812. doi:10.1038/nsmb.2061

van Westen R, Poppinga J, Díez Arazola R, Toonen RF, Verhage M. 2021. Neuromodulator release in neurons requires two functionally redundant calcium sensors. *Proc Natl Acad Sci* **118**:1–12. doi:10.1073/pnas.2012137118

Vevea JD, Chapman ER. 2020. Acute disruption of the synaptic vesicle membrane protein synaptotagmin 1 using knockoff in mouse hippocampal neurons. *Elife* **9**:1–24. doi:10.7554/eLife.56469

Wolfes AC, Dean C. 2020. The diversity of synaptotagmin isoforms. *Curr Opin Neurobiol*. doi:10.1016/j.conb.2020.04.006

Xu J, Mashimo T, Südhof TC. 2007. Synaptotagmin-1, -2, and -9: Ca2+ Sensors for Fast Release that Specify Distinct Presynaptic Properties in Subsets of Neurons. *Neuron* **54**:567–581. doi:10.1016/j.neuron.2007.05.004

Xu J, Pang ZP, Shin OH, Südhof TC. 2009. Synaptotagmin-1 functions as a Ca2+ sensor for spontaneous release. *Nat Neurosci* **12**:759–766. doi:10.1038/nn.2320

Yao J, Kwon SE, Gaffaney JD, Dunning FM, Chapman ER. 2012. Uncoupling the roles of synaptotagmin I during endo- and exocytosis of synaptic vesicles. *Nat Neurosci* **15**:243–249. doi:10.1038/nn.3013

Zhou Q, Zhou P, Wang AL, Wu D, Zhao M, Südhof TC, Brunger AT. 2017. The primed SNARE-complexin-synaptotagmin complex for neuronal exocytosis. *Nature* **548**:420–425. doi:10.1038/nature23484

METHODS

Animals

All neuronal cultures were prepared from early postnatal (P0-P1) mice in accordance with all relevant regulations and the approval of the University of Wisconsin Institutional Animal Care

and Use Committee. Conditional *Syt9 KO* mice were obtained from Jackson Labs (Xu et al. 2007). These conditional *Syt9* KO mice were terminally crossed with an E2a-CRE mouse (Jackson Labs) to yield a population of constitutive *Syt9* KO mice; the mice used in this study are all products of this constitutive *Syt9* KO mouse. *Syt1* cKO (conditional KO) mice were a gift from W. Thoreson, (University of Nebraska-Lincoln; (Quadros et al., 2017)).

Genotyping

The *Syt9* KO mouse line was maintained by double heterozygous breeders so that offspring WT and KO littermates could be studied. To genotype the neonatal pups, tissue samples were taken by collecting ~2 mm of the end of the tail and then extracting DNA from the tissue sample with Kapa Express Extract Kit (Roche). The extracted DNA was then subjected to PCR using in-house designed primers to identify WT and KO alleles. The primers used to identify the WT allele yield a 209 bp amplicon: F-primer 5'-GCGTCAATGGGAGGAGAGGTCA-3'; R-primer 5'-GTCCACTAGGGCTAGCCCAGG-3'. The primers used to identify the KO allele yield a 301 bp amplicon: F-primer 5'-CAGTAGGGAGCGAGCAGAAATTAAAAT-3'; R-primer 5'-AACTTCGTCGATCGACCTCGAATAA-3'. The PCR product was subjected to agarose gel electrophoresis and imaged on a ChemiDoc MP imaging system (BioRad).

Molecular biology and lentiviral preparation

Lentiviral vectors were based on a modified FUGW (FUGW was a gift from David Baltimore [Addgene plasmid # 14883; http://n2t.net/addgene:14883; RRID: Addgene_14883]) (Lois et al., 2002). The FUGW vector was modified by substituting the ubiquitin promoter with the human synapsin I promoter (Kügler et al., 2003); this vector is henceforth referred to as FSGW. pH-SYT9 was generated by replacing SYT1 in pHluorin-SYT1 (a gift from T.A. Ryan, Weill Medical College of Cornell University, New York, NY) (Kim and Ryan, 2009) with a SYT9 cDNA (a gift from M. Birnbaum, University of Pennsylvania, Philadelphia, PA) [(Hudson and Birnbaum, 1995); note: SYT9 is referenced in this study as SYT5], using PCR splicing via overlap extension (SOE). The pHluorin-SYT9 cassette replaced GFP in the cloning site of the FSGW vector via In-Fusion Cloning (Takara Bio). The SP-pH construct was generated by PCR SOE and comprised: the first 68 residues of mouse preprotachykinin (PPT), a $GS(GSS)_4$ linker, and a super-ecliptic pHluorin (Miesenböck et al., 1998). This fusion construct was subcloned into FSGW.

SYT9 CLM constructs correspond to D>N substitutions of two calcium ligands in each C2-domain as follows: $C2A_m$; D197N and D199N; $C2B_m$; D330N and D332N. All four mutations are present in the $C2A_mB_m$ construct. These constructs were made by performing site-directed mutagenesis on the *Syt9* cDNA with the QuikChange Lightning Site-Directed Mutagenesis Kit (Agilent). Full-length CLM constructs were used for the rescue experiments in Fig. 7, and isolated purified C2 domain CLM constructs were used for Fig. 6. cDNA for SNAP-25B was provided by M. C. Wilson (University of New Mexico School of Medicine, Albuquerque, NM), and full-length synaptobrevin 2 (SYB2) and syntaxin 1A (SYX) were provided by J. E. Rothman (Yale University, New Haven, CT); these SNARE proteins were subcloned into pTrcHis vectors to yield His_6-tagged proteins (Evans et al., 2015).

Cell culture, transient transfection, and lentiviral transduction

Cortical, hippocampal, and striatal regions were obtained by microdissection and kept in ice-cold Hibernate-A (BrainBits) with 2% B-27 until completion of dissection. Neural tissue was then incubated with trypsin-EDTA (Corning, 0.25%) for 25 minutes at 37°C. The tissue was washed with DMEM (Gibco) supplemented with FBS and Penicillin-streptomycin and triturated 10-15 times with a P1000 pipette tip until complete dissociation of the tissue. Cells were plated at a density of 100,000 cells/cm^2 onto poly D-lysine-coated glass coverslips. For SP-pH release experiments, Supplemented DMEM was replaced after 1 hour with Neurobasal-A (Gibco) supplemented with B-27 and GlutaMAX. For SP-pH release experiments, sparse transfection of SP-pH and a cytosolic mRuby marker was required for identifying and imaging single neurons. This was achieved using Lipofectamine LTX (Invitrogen) on DIV 8-9. For localization studies, rescue experiments, and Ca^{2+} imaging, full coverage was desirable and was achieved via lentiviral transduction. Lentivirus encoding CRE-recombinase was added to *Syt1* cKO neurons at DIV 0-2, and lentiviruses that expressed SYT9 rescue constructs, the calcium imaging construct synaptophysin-HaloTag (SYP-Halo) (Bradberry and Chapman, 2022), or SP-pH for localization studies, were added to neurons at DIV 5-7.

Electrophysiological studies

Whole-cell voltage-clamp recordings of cultured neurons (DIV14-18) were performed at room temperature in artificial CSF containing (in mM): 128 NaCl, 5 KCl, 1.5 $CaCl_2$, 1 $MgCl_2$, 30 glucose, 25 HEPES-NaOH, with an internal solution containing (in mM): 130 KCl, 10 HEPES-NaOH, 1 EGTA, 2 ATP, 0.3 GTP, 5 phosphocreatine. Recordings were performed using a MultiClamp 700B amplifier and Digidata 1550B digitizer (Molecular Devices) under the control of Clampex 10 software (Molecular Devices). $GABA_A$-mediated currents were pharmacologically isolated using CNQX (20 µM) and D-AP5 (50 µM) in the bath solution; for mIPSC recordings, tetrodotoxin (1 µM) was included in the bath. QX 314 chloride (5 mM) was included in the pipette solutions for all recordings. Neurons were held at -70 mV in all experiments without correction for liquid junction potentials. Series resistance was monitored, and recordings were discarded if this quantity rose above 15 MΩ. For evoked recordings, a concentric bipolar electrode (FHC, 125/50 um extended tip) was placed 100-200 um away from the patched soma and stimulation currents were adjusted to evoke maximal responses. For mIPSC recordings, 300 seconds of data were recorded for each striatal neuron, and 180 seconds of data were acquired for cortical and hippocampal neurons. mIPSCs were quantified for each recording using a template-matching algorithm in Clampfit (Molecular Devices). For pharmacology rescue experiments, peptides and analogs were added to the ACSF at 100 nM, except for SR140333, which was added at 10 nM. Neurons were incubated in these for ten minutes before patch-clamp experiments were carried out.

Immunoblotting

Coverslips of neurons (DIV 14-18) were rinsed 1-2 times in PBS and lysed by repeated pipetting of lysis buffer (50 mM Tris pH 8.0, 150 mM NaCl, 2% SDS, 0.1% Triton X-100, 10 mM EDTA) containing a protease inhibitor cocktail (cOmplete mini EDTA-free, Roche, 1 tablet / 10 mL lysis buffer). For quantitative Western blots of lysates, protein concentration was determined using a bicinchoninic acid (BCA) assay (Thermo Scientific) to ensure equal amounts of protein were subjected to SDS-PAGE. Samples were then combined with 4X Laemmli sample buffer, heated

to 50°C for 15 minutes, and stored at -20°C until use. For each immunoblot experiment, the samples were subjected to SDS-PAGE 13% polyacrylamide gels containing 1% trichloroethanol (TCE). After electrophoresis, the TCE was activated by exposure to UV light (300 nm) for 45 seconds, and labeled proteins were detected via 300 nm illumination; these signals served as a protein loading control (Ladner et al., 2004). Proteins were transferred to a PVDF membrane, which was then blocked with 5% nonfat milk in Tris-buffered saline plus 0.1% Tween 20 (TBST) for 1 hour, followed by incubation with primary antibody overnight at 4°C. Blots were then washed 3 times for 5 minutes in TBST, incubated with secondary antibody for 1 hour, and washed again as above. For the pH-SYT9 rescue experiments, after blotting for SYT9, the PVDF membranes were stripped using Restore™ Western Blot Stripping Buffer (Thermo), and the membranes were once again blocked and subsequently probed for SYT1. Primary antibodies were: α-SYT1 (1:500) (DSHB; #mAB 48; RRID:AB_2199314) and α-SYT9 (1:500) (Synaptic Systems Cat# 105 053, RRID:AB_2199639). Secondary antibodies were: goat α-mouse IgG-HRP (Biorad, 1706516; RRID:AB_11125547), goat α-mouse IgG2b-HRP (Invitrogen, M32407; RRID:AB_2536647), and goat α-rabbit IgG-HRP (Biorad, 1706515, RRID:AB_11125142). Immunoreactive bands were visualized using SuperSignal West Pico Plus Chemiluminescent Substrate (Thermo) and imaged with an Amersham Imager 680 imaging system (GE Healthcare). Bands were analyzed by densitometry, with care to stay within the linear range, and contrast was linearly adjusted for publication using ImageJ (Fiji)(Schindelin et al., 2012).

Immunocytochemistry and confocal microscopy

Immunocytochemistry was carried out as previously described (Courtney et al., 2019). For the pH-SYT9 rescue experiments, immediately before fixation and permeabilization, cortical neurons were incubated in primary antibody directed against the pHluorin tag of pH-SYT9 (1:250) (α-GFP; rabbit polyclonal; Abcam Cat# ab290, RRID: AB_303395) in culture medium to label only the surface-resident pH-SYT9, as the antibody is unable to enter intact, live neurons. After fixation and permeabilization, the neurons were incubated a second time with primary antibodies to label synaptophysin (1:1000) (α-SYP; guinea pig polyclonal; SySy; 101 004; RRID:AB_1210382) and pHluorin (1:1000) (α-GFP; chicken monoclonal; Abcam Cat# ab13970, RRID:AB_300798). This second α-GFP antibody labeled all pHluorin tags that were not labeled by the first α-GFP ‘blocking’ antibody, to reveal the internal fraction of pH-SYT9. This strategy allowed for differential secondary labeling of the different pH-SYT9 populations with species-specific secondary antibodies conjugated to small-molecule dyes.

Images were acquired on a Zeiss LSM 880 laser scanning confocal microscope with a 63x Plan-Apochromat 1.4NA DIC oil immersion objective. Identical laser and gain settings were used for all samples within each experimental paradigm. Images were analyzed in ImageJ (Fiji)(Schindelin et al., 2012), and the Coloc2 plugin was used for colocalization analysis. For synapse counting experiments, images were exported to SynD (Schmitz et al., 2011), where MAP2 staining was used to create a neurite mask, then synapse number was quantified by counting the number of overlapping VGAT and Gephyrin puncta within the neurite mask. Primary antibodies were: α-GFP (1:1000) (Abcam Cat# ab290, RRID:AB_303395), α-GFP (1:1000) (Abcam Cat# ab13970, RRID:AB_300798), α-SYT1 (1:500) (DSHB; #mAB 48; RRID:AB_2199314), α-SYP (1:1000) (Synaptic Systems Cat# 101 004; RRID:AB_1210382), α-

SYT9 (1:500) (Synaptic Systems Cat# 105 053, RRID:AB_2199639), α-CHGB (Synaptic Systems Cat# 259 103; RRID:AB_2619973), α-VGAT (1:1000)(Synaptic Systems Cat # 131 004; RRID:AB_887873), α-Gephyrin (1:1000)(OriGene Cat# TA502313, RRID:AB_11126039), and α-MAP2 (1:500) (Abcam Cat# ab5392, RRID:AB_2138153). Secondary antibodies were: goat anti-chicken IgY-Alexa Fluor 405 (1:500) (abcam; ab175675, RRID:AB_2810980), goat α-chicken IgY-Alexa Fluor 488 (1:500) (Thermofisher A-11039, RRID: AB_2534096), goat α-guinea pig IgG-Alexa Fluor 488 (1:500) (Thermofisher; A-11073; RRID:AB_2534117), goat α-rabbit IgG-Alexa Fluor 546 (1:500) (Thermofisher; A-11010, RRID:AB_2534077), goat α-guinea pig IgG-Alexa Fluor 647 (1:500) (Thermofisher; A-11074, RRID:AB_2534118), and goat α-mouse IgG2b-Alexa Fluor 647 (1:500) (Thermofisher; A-21242; RRID:AB_2535811).

Live cell imaging

DIV 14-18 striatal neurons were washed twice in ASCF before being mounted in an imaging chamber with parallel platinum electrodes (Warner Instruments, Hamden, CT, USA) with 500 µl of ACSF. Imaging was carried out with a 40x, 1.4 NA oil-immersion objective on an inverted epifluorescence microscope (IX81, Olympus, Tokyo, Japan) equipped with a CMOS camera (Orca Flash 4.0 V2, Hamamatsu Photonics, Hamamatsu, Japan), motorized stage (Mad City Labs, Madison, WI, USA), and a custom illumination source containing three LEDs (470, 530, 625 nm) (Thorlabs, Newton, NJ, USA). The system was controlled using Micro-Manager (Edelsteinet al. 2010). Stimulation was delivered with a stimulation box (SD9, Grass Instrument Co., West Warwick, RI, USA) controlled via a HEKA EPC10 DAQ-amplifier and PatchMaster software (HEKA, Holliston, MA, USA), which was also used to synchronize the start of image sequence acquisition. Images were collected using 2 x 2 binning (0.365 µm x 0.365 µm pixel size).

For SP-pH release imaging, an exposure time of 100 ms was used. Individual transfected neurons were identified for imaging by first detecting the cytosolic mRuby signal with the 530 nm LED and standard RFP filter set. SP-pH release was imaged with the 470 nm LED, a standard green fluorescent protein (GFP) filter set (49002, Chroma, Bellows Falls, VT, USA). Ten seconds of baseline were first obtained before stimulation was given 16 periods of 50 APs at 50 Hz with 0.5 sec between each train. Seventy seconds after the start of stimulation, 500 µl of 2x NH_4Cl ACSF, containing (in mM): 100 NH_4Cl, 28 NaCl, 5 KCl, 1.5 $CaCl_2$, 1 $MgCl_2$, 30 glucose, 25 HEPES, pH 7.4, was added to dequench pHluorin fluorescence to visualize the total number of SP-pH-bearing vesicles.

For Ca^{2+}-imaging, the 625 nm LED, custom three-band pass dichroic mirror (Chroma) and far-red emission filter, and a 10 ms exposure time were used. DIV 14-18 striatal neurons that were transduced with a virus that induced expression of SYP-Halo were washed twice in ACSF before and then incubated in ACSF containing 100 nM of the acetoxymethyl ester of JF_{646}-BAPTA bearing a HaloTag ligand (JF_{646}-BAPTA-AM-HTL)(Deo et al., 2019), a gift from L. Lavis (Janelia Research Campus). After a 20-minute incubation at 37°C, the cells were again washed with dye-free ACSF and incubated for 20 minutes at 37°C before being mounted in the imaging chamber. Five fields of view (FOV) were selected per coverslip. Three seconds of baseline were recorded before one 0.6 ms stimulus was given, and then a saturating stimulus (50 AP @ 50Hz) was delivered to establish a maximum fluorescence (F_{max}) for each field of view.

Image analysis

For colocalization analysis, Fiji was used. The Coloc2 plugin was used to determine the Mander's Correlation coefficients and Pearson's correlation coefficients; Costes' automatic threshold was used for both determinations.

For SP-pH release analysis, Fiji with the DCV_pHluorin toolset (https://github.com/alemoro/DCVpHluorin_toolseet) (Moro et al., 2021) was used; 3 pixels x 3 pixels regions of interest (ROIs) were placed over each observed increase in fluorescence, and somatic events were excluded. Fusion events were defined as a sudden increase of 1.25 SD above the average fluorescence of the first 100 frames in the ROI (F_0). Time lapses were also manually scored along with the DCV_pHluorin analysis algorithm to ensure a thorough and complete characterization of each release event. Pool size estimations were calculated using the same rules used for fusion event detection, after perfusion with NH_4Cl. Analysis was blinded, and the number of fusion events, SP-pH vesicle pool size estimation, event duration, and fusion onset timing were all determined using DCV_pHluorin. Output data were processed in Excel and plotted using GraphPad Prism.

Ca^{2+}-imaging analysis was performed as previously described (Bradberry and Chapman, 2022; Vevea and Chapman, 2020). Briefly, SYP-HaloTag-JF_{646}-BAPTA traces were background subtracted, and ROIs were created based on a custom workflow to identify changes in fluorescence of the selected image series. An average projection (created using the pre-stimulus fluorescence baseline) was subtracted from the maximum projection (created using the entire image series). This result was duplicated and mean filtered using a rolling ball radius of 10 pixels. These images were subtracted, and the result was used to threshold changes in fluorescence. After thresholding, images were made binary and a watershed function was run to separate objects that slightly overlapped. Using this procedure, objects (>10 pixels) were created and ROIs were defined. These ROIs were used to measure fluorescence changes over time from the original image series. The fluorescence traces of each ROI were then imported into AxoGraph where the basal, pre-stimulation fluorescence of each ROI (F_r) was subtracted from the max fluorescence at indicator saturation (F_{max}) to give a ΔF. The following equation was used:

$$[Ca^{2+}]_i = K_d \left(\frac{F_r/F_{max} - 1/R_f}{1 - F_r/F_{max}} \right)$$

where K_d is the dissociation constant of the indicator, F_r is the baseline fluorescence of an ROI pre-stimulation, F_{max} is the fluorescence achieved with the delivery of a saturating stimulus, R_f is the dynamic range of the indicator, and n is the Hill coefficient. For K_d, R_f and n, we used *in vitro* measurements (K_d = 140 nM, R_f = 5.5, n = 1) from (Deo et al., 2019).

Trafficking analysis was carried out using the Multi Kymograph plugin in Fiji; 30-second time-lapses, taken after NH_4Cl perfusion in the SP-pH release experiments, were used. Ninety µm segments that began within 20 µm of the soma were chosen. The kymograph was created from this time-lapse and every path was traced and quantified.

Protein Purification

Recombinant proteins were made as described (Evans et al., 2015). SYB2, SNAP-25B, and SYX were purified as His_6-tagged proteins using the pTrcHis vector. The SYT1 cytoplasmic domain (SYT1 C2AB – residues 96-421; the amino acid residues of the other SYT constructs are indicated in parentheses), SYT1 C2A (96-264), and SYT1 C2B (248-421), were purified as GST-tagged proteins using a pGEX vector. The SYT9 cytoplasmic domain (SYT9 C2AB –104-386), SYT9 C2A (124-211), and SYT9 C2B (253-344) were purified as His_6-tagged proteins using the pTrcHis vector. Isolated SYT9 C2A and C2B domains, harboring Ca^{2+}-ligand mutations, were purified in the same manner at the WT C2-domains. Full-length SYT9 was purified as a His_6-SUMO-tagged protein using the pET28 vector.

Vesicle Preparation

Protein free liposomes, for co-sedimentation assays, were generated by drying lipids (30% PE and 70% PC; 15% PS, 30% PE, and 55% PC; and 25% PS, 30% PE, and 45% PC) in chloroform, under a stream of nitrogen. The film was rehydrated and suspended by vortexing in 50 mM HEPES-NaOH, 100 mM NaCl, pH 7.4, and extruded through 50 nm polycarbonate membranes to generate liposomes (Avanti Polar Lipids). SNARE-bearing vesicles, for *in vitro* fusion assays, were prepared as previously described (Bhalla et al., 2006). Lipid compositions were as follows: 15% PS, 27% PE, 55% PC, 1.5% NBD-PE, and Rho-PE for SYB2 vesicles, and 25% PS, 30% PE, and 45% PC for SYX1A vesicles.

***In vitro* Fusion Assays**

Fusion assays between SYB2 and SYX1A vesicles were carried out in a scaled-down version of the referenced method (Bhalla et al., 2006). For split t-SNARE fusion assays, 1 μM of the cytoplasmic domain (C2AB) or 2 μM of isolated C2-domains, SYB2 vesicles, SYX1A vesicles, 0.2 mM EGTA, and 7 μM soluble SNAP-25B were incubated for 20 min at 37°C. Ca^{2+} (1 mM final free concentration) was added and the reaction was monitored for an additional 60 min. N-dodecyl-β-d-maltoside was added at the end of the experiment, to yield the maximum fluorescence signal. NBD donor fluorescence was monitored using a Synergy HT multi-detection microplate reader (Bio-Tek). Traces were normalized to the first time point, and the maximum fluorescence signal, to determine the $\%F_{max}$.

Co-sedimentation Assays

WT SYT9 C2A, C2B, or C2AB (4 μM) were combined with protein-free liposomes (1 mM total lipid; %PS as indicated in Fig. 6B) in 0.2 mM EGTA or 1 mM Ca^{2+} and incubated for 15 min at RT. Samples were then centrifuged in an Optima MAX-E tabletop ultracentrifuge (Beckman Coulter) at 184,000 x g (65,000 rpm) for 45 min at 4°C. After centrifugation, the supernatant (S) and the pellet (P) were collected, and equal fractions were subjected to SDS-PAGE and Coomassie blue staining. Bands were quantified by densitometry and plotted.

Isothermal Titration Calorimetry (ITC)

WT and Ca^{2+} ligand mutant forms of the isolated C2-domains of SYT9 were dialyzed overnight in ITC buffer (50 mM HEPES-NaOH, pH 7.4, 200 mM NaCl, and 10% glycerol) in the presence of Chelex-100 resin (BioRad), to remove residual divalent cations. ITC buffer was subsequently filtered and used to make Ca^{2+} and protein dilutions. Heat of binding was measured, using a

MicroCal® iTC200 (Malvern), at 25 °C, in response to twenty injections of Ca^{2+} into the sample cell containing 100 µM protein. Heat of dilution was corrected by subtracting the signal that arises when Ca^{2+} is diluted into buffer. Data were analyzed using the "sequential binding site" model in the data software package.

COMPETING INTERESTS

The authors have no competing interests to declare.

ACKNOWLEDGEMENTS

We would like to thank members of the Chapman lab and K. Bjornson for insightful comments and valuable discussion related to the manuscript. This study was supported by grants from the NIH (MH061876 and NS097362 to ERC). MJS was supported in part by the UW-Madison Neuroscience Training Program Training Grant (T32 NS105602). CSE was supported in part by a PhRMA Foundation predoctoral fellowship and by the UW-Madison Molecular and Cellular Pharmacology Training Grant (T32 GM008688). ERC is an Investigator of the Howard Hughes Medical Institute.

FIGURE LEGENDS

Figure 1. SYT9 is expressed in cultured cortical, hippocampal, and striatal neurons but does not support evoked neurotransmitter release. a, Immunoblot of DIV14 cortical (CTX), hippocampal (HIP), and striatal (STR) neuronal lysates from *Syt1* cKO mice +/- CRE lentivirus; recombinant SYT1 C2AB served as a standard to quantify SYT1 expression levels. TCE staining served as a loading control. **b**, Quantification of the SYT1 expression levels in each of the three neuronal lysates, as a fraction of total protein (n = 6). **c**, Representative evoked IPSC (eIPSC) traces from *Syt1* cKO striatal neurons +/- CRE, and (**d**) peak eIPSC amplitudes from - CRE (n = 21) or + CRE (n = 22) cells, showing loss of synchronous release upon loss of SYT1 ($p < 0.0001$; Mann-Whitney test). **e**, Same as panel (**a**) but blotting for SYT9 in the lysates, using the indicated amounts of a full-length recombinant SYT9 standard; SYT9 is expressed at ~25-fold lower levels than SYT1. **f**-**h**, Same as panels (**b**-**d**), but for SYT9 expression (n = 4) (**f**) and WT (n = 28) *Syt9* KO (n = 27) striatal neurons (**g**-**h**). In sharp contrast to *Syt1* cKO neurons, loss of SYT9 did not affect single eIPSCs in striatal neurons ($p = 0.6979$; unpaired Student's t-test). For all figures *$p < 0.05$, **$p < 0.01$; ***$p < 0.001$; ****$p < 0.0001$; ns indicates $p > 0.05$, and error bars represent SEM.

Figure 2. SYT9 rescues SYT1 KO phenotypes only when over-expressed. a, Immunoblots of DIV14 cortical neuronal lysates from *Syt1* cKO mice, with or without addition of CRE lentivirus. TCE staining served as a loading control. + CRE neurons were later transduced with lentivirus encoding pHluorin-tagged SYT9 (pH-SYT9), resulting in either a 1-fold or 25-fold degree of over-expression as compared to endogenous SYT9. A closed arrowhead indicates endogenous SYT9 bands, an open arrowhead indicates pH-SYT9 bands, and ~ indicates proteolysis product bands. Representative eIPSC traces (**b**), average amplitudes (**c**), and time-to-peak (**d**), are plotted for - CRE (n = 21), + CRE (n = 19), + CRE +1x pH-SYT9 (n = 25), and + CRE +25x pH-SYT9 (n = 23) conditions. SYT9 partially rescued eIPSC amplitude, but only

when over-expressed 25-fold; the synchronicity of release was partially rescued at one-fold over-expression and was fully rescued at 25-fold over-expression of SYT9. **e**, Representative miniature IPSC (mIPSC) traces, showing increased rates of mIPSCs in *Syt1* cKO (n = 10) neurons compared to WT (n = 12). One-fold over-expression of SYT9 was without effect (n = 16); full rescue of the unclamped phenotype was observed at 25-fold over-expression (n = 15); these data are quantified in (**f**). **g**, mIPSC amplitude was not affected under any condition tested. **h**, Representative immunofluorescence images of cultured *Syt1* cKO cortical neurons +/- CRE, with and without over-expressed pH-SYT9. Rescue constructs were tagged at the N-terminus with a pHluorin to enable differential labeling of the surface and internal fractions using α-GFP antibodies, see Methods for details. pH-SYT9 was present in both the plasma membrane (red) and on internal compartments (green). Synaptic vesicles were marked using an α-synaptophysin (SYP) antibody (magenta). **i**, Quantification of the colocalization between synaptophysin and: internal pH-SYT9, endogenous SYT1, and endogenous SYT9. In this figure, stars (*) indicate statistical comparisons (one-way ANOVA with Šídák's multiple comparisons test) to *Syt1* cKO neurons without CRE; hash symbols (#) indicate statistical comparisons to *Syt1* cKO neurons + CRE, where #p < 0.05, ##p < 0.01; and ###p < 0.001; and ####p < 0.0001.

Figure 3. SYT9 KO striatal neurons display decreased mIPSC frequency. a, Representative mIPSCs traces recorded from WT (n = 33), *Syt9* KO (n = 29), and *Syt9* KO + WT (n = 24) striatal neurons. **b**, Overlay of averaged mIPSCs from the three above conditions, revealing no change in kinetics or amplitude. c, mIPSC frequency is reduced in *Syt9* KO striatal neurons and this was rescued via re-expression of SYT9 using lentivirus.

Figure 4. SYT9 regulates the secretion of substance P-pHluorin from striatal neurons. a, Representative images of cultured striatal neurons stained with α-SYT9 antibodies (magenta), α-GFP (SP-pHluorin) (green); channels are merged on the right. **b**, SYT9 is co-localized with SP-pH, and vice versa; quantification was carried out using the Mander's correlation coefficient. **c**-**d**, As in panels (**a-b**) but co-stained with α-CHGB (magenta) and α-GFP antibodies (green). SP-pH is co-localized with CHGB, confirming that SP-pH is targeted to DCVs. **e**, schematic of the SP-pH release assay. **f**, Representative traces of individual SP-pH vesicle fusion events; the stimulation paradigm is overlaid in red, and alkalinization of DCVs with NH_4Cl is shown in green. **g**, The released fraction of SP-pH is reduced in *Syt9* KO neurons (n = 27) compared to WT (n = 21) (p = 0.0049; Mann-Whitney test). **h**, Pool size per neuron was unchanged in *Syt9* KO neurons (p = 0.60). **i**, Plot of cumulative SP-pH fusion events; again the stimulus protocol is indicated in red. **i**, Histogram of SP-pH release event duration for WT and SYT9 KO striatal neurons.

Figure 5. Treatment with substance P rescues SYT9 KO mIPSC phenotype. a, Representative mIPSC traces recorded from striatal neurons as follows: WT (n = 35); *Syt9* KO (n = 39); WT with application of 2 µM substance P (n = 28) or 100 nM SR140333 (n = 34); SYT9 KO with application of either: 2 µM substance P (n = 35), 2 µM GR73632 (n = 18), 2 µM Leu-enkephalin (n = 23), 2 µM dynorphin A (n = 23), or 2 µM cholecystokinin (n = 20) in the bath solution. **b**-**c**, Average amplitude (**b**) and frequency (**c**) of mIPSCs recorded from (**a**). We reiterate that the asterisk (*) indicates statistical comparisons (one-way ANOVA with Šídák's

multiple comparisons test) to WT neurons; hash symbols (#) indicate statistical comparisons to *Syt9* KO neurons. **p < 0.01; ***p < 0.001; ****p < 0.0001; ###p < 0.001 and ####p < 0.0001.

Figure 6. Ca^{2+}•C2A from SYT9 regulates membrane fusion *in vitro*. a, *Left panel:* Reconstituted split t-SNARE fusion assay where Ca^{2+}•SYT fragments must fold soluble SNAP-25B onto reconstituted SYX1A for fusion with SYB2 proteoliposomes to occur. Representative fusion traces, using each isolated C2-domain, C2A and C2B, from SYT1 and SYT9 are shown (left); the tandem C2-domains, C2AB, for each isoform were also assayed in parallel but were omitted from the left panel for clarity. The isolated C2A domain, but not the C2B domain, of SYT9 stimulated fusion; in SYT1, C2B, rather than C2A, stimulated fusion (Gaffaney et al., 2008). *Right panel*: The extent of fusion (80 min), using all SYT constructs, in the presence (+) or absence (-) of Ca^{2+}, is plotted (n ≥ 3). **b**, Binding of SYT9 C2A, C2B, and C2AB to PS-bearing liposomes was monitored via a co-sedimentation assay. Representative SDS-PAGE gels of protein from equal fractions of the supernatant (S), and pellet (P), as well as the total input (T), in the absence (0.2 mM EGTA) or presence of Ca^{2+} (1 mM free), using liposomes with 0, 15 and 25% PS, are shown (left). Protein band intensities were normalized to the total input and plotted (right; n ≥ 3). **c**, Representative ITC traces showing the heat of Ca^{2+} binding to the isolated C2-domains of WT and Ca^{2+}-ligand mutant (CLM) forms of SYT9; (n = 4). Thermodynamic values are provided in Supplementary Table 2.

Figure 7. The Ca^{2+}-binding activity of the C2A domain of SYT9 is required for its action in neurons. a, Representative mIPSC traces recorded from striatal neurons as follows: WT (n = 20), *Syt9* KO (n = 17), *Syt9* KO + WT rescue (n = 24), *Syt9* KO + $C2A_m$ rescue (n = 19), *Syt9* KO + $C2B_m$ rescue (n = 20), and *Syt9* KO + $C2A_mB_m$ (n = 19) rescue. **b**-**c**, Average frequency (**b**) and amplitude (**c**) of mIPSCs recorded from (**a**). WT SYT9 and $C2B_m$ mutant rescued the mini frequency, while the $C2A_m$ and $C2A_mB_m$ mutants failed to rescue this phenotype.

Figure 8. SYT9 indirectly controls MSN synaptic transmission by serving as a Ca^{2+} sensor for SP exocytosis. a, A model in which SYT9 serves as a Ca^{2+} sensor that regulates the exocytosis of SP-containing DCVs from striatal neurons. Released then SP activates the NK1 receptor which in turn activates the IP_3 pathway via $G_{q/11}$ and PLC, leading to increased Ca^{2+} efflux from the ER, to drive spontaneous neurotransmitter release.

SUPPLEMENTAL MATERIALS

Supplementary Table 1

Thermodynamic properties of Ca^{2+} binding to the isolated C2A and C2B domains of SYT9 as determined using ITC. Representative traces of SYT9 C2-domain•Ca^{2+} titrations are shown in Figure 5C. Data presented as mean ± SEM, *n* = 4.

Supplemental Figure 1. SYT1, but not SYT9, supports evoked neurotransmitter release in cortical and hippocampal neurons. a-**b***,* Representative traces of eIPSCs recorded from WT and *Syt9 KO* cortical (WT n = 26; KO n = 17) (**a**) and hippocampal (WT n = 23; KO n = 22) (**b**) neurons with quantification of peak eIPSC amplitude. **c**-**d**, Same as a-b, but using *Syt1* cKO

neurons; cortical neurons (WT n = 20; KO n = 23); hippocampal neurons (WT n = 22; KO n = 26).

Supplemental Figure 2. Synaptic depression is unchanged in *Syt9* KO cortical, hippocampal, and striatal neurons. a, Representative 10 Hz eIPSC traces from WT (n = 21) and *Syt9* KO (n = 21) cortical neurons. **b**, Quantification of peak amplitudes from each pulse normalized to the first pulse, showing no difference in short-term plasticity. **c**-**d**, Same as **a**-**b**, but with hippocampal neurons (WT n = 17; KO n = 17). **e**-**f**, Same as **a**-**b**, but with striatal neurons (WT n = 35; KO n = 38). Error bars indicate SEM.

Supplemental Figure 3. eIPSC charge transfer and decay kinetics of *Syt1* cKO cortical neurons expressing pH-SYT9. a, Plot of normalized cumulative charge transfer of - CRE, + CRE, + CRE + 1x pH-SYT9, and + CRE + 25x pH-SYT9 conditions. **b**, Plot of mean decay time (90%-10%) for each condition; 25x fully rescues the decay time, while 1x fails to rescue. Further decay analysis was not performed due to receptor-dominated decay kinetics of IPSCs in cultured neurons. In this figure, stars (*) indicate statistical comparisons (one-way ANOVA with Šídák's multiple comparisons test) to *Syt1* cKO neurons without CRE; hash symbols (#) indicate statistical comparisons to *Syt1* cKO neurons + CRE, where ##p < 0.01.

Supplemental Figure 4. mIPSC frequency is unaltered in *Syt9* KO cortical and hippocampal neurons. a, Representative mIPSC traces recorded from WT (n = 27) and *Syt9* KO (n = 22) cortical neurons. **b**, mIPSC frequency was unaltered in *Syt9* KO cortical neurons. **c**, Overlay of averaged mIPSCs, revealing no change in kinetics or amplitude. **d**-**f**, Same as **a**-**c**, but using hippocampal neurons (WT n = 24; KO n = 27).

Supplemental Figure 5. Synaptic density was unchanged in *Syt9* KO striatal neurons. a, Representative images of cultured WT (n = 15) and *Syt9* KO (n = 15) striatal neurons stained with α-Gephyrin (red) and α-VGAT (green) antibodies with a neurite mask generated from MAP2 staining (magenta). Gephyrin and VMAT overlap within the neurite mask were counted (purple puncta within synapse mask). Scale bars represent 20 µm. **b**, Number of synapses per µm is unaltered in cultured *Syt9* striatal neurons.

Supplemental Figure 6. The trafficking of SP-pH-bearing DCVs is unaltered in *Syt9* KO striatal neurons. a, *Upper panel*: Representative image of a 90 µm region of a striatal neuron transfected with SP-pH after NH_4Cl perfusion. *Lower panels*: Kymograph of this region; each track in the kymograph was traced and quantified in the bottom panel (yellow lines). **b**, Quantification of the displacement and direction of SP-pH vesicles. No significant differences in WT (n = 98 vesicles) versus *Syt9* KO (n = 101 vesicles) striatal neurons were detected.

Supplemental Figure 7. Basal presynaptic [Ca^{2+}] is unchanged in *Syt9* KO striatal neurons. a, Three seconds of baseline was recorded before a high-frequency stimulation was delivered to obtain maximal fluorescence of the indicator which allows for calculation of resting $[Ca^{2+}]_i$ (see Methods). **b**, Resting presynaptic $[Ca^{2+}]_i$ in 1.5 mM $[Ca^{2+}]_e$ did not differ between WT (n = 45) and *Syt9* KO (n = 44) striatal neurons.

FIGURE 1

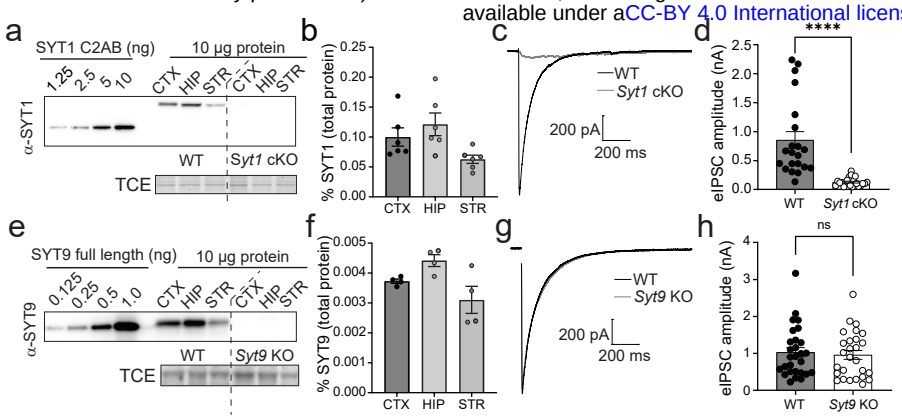

FIGURE 2

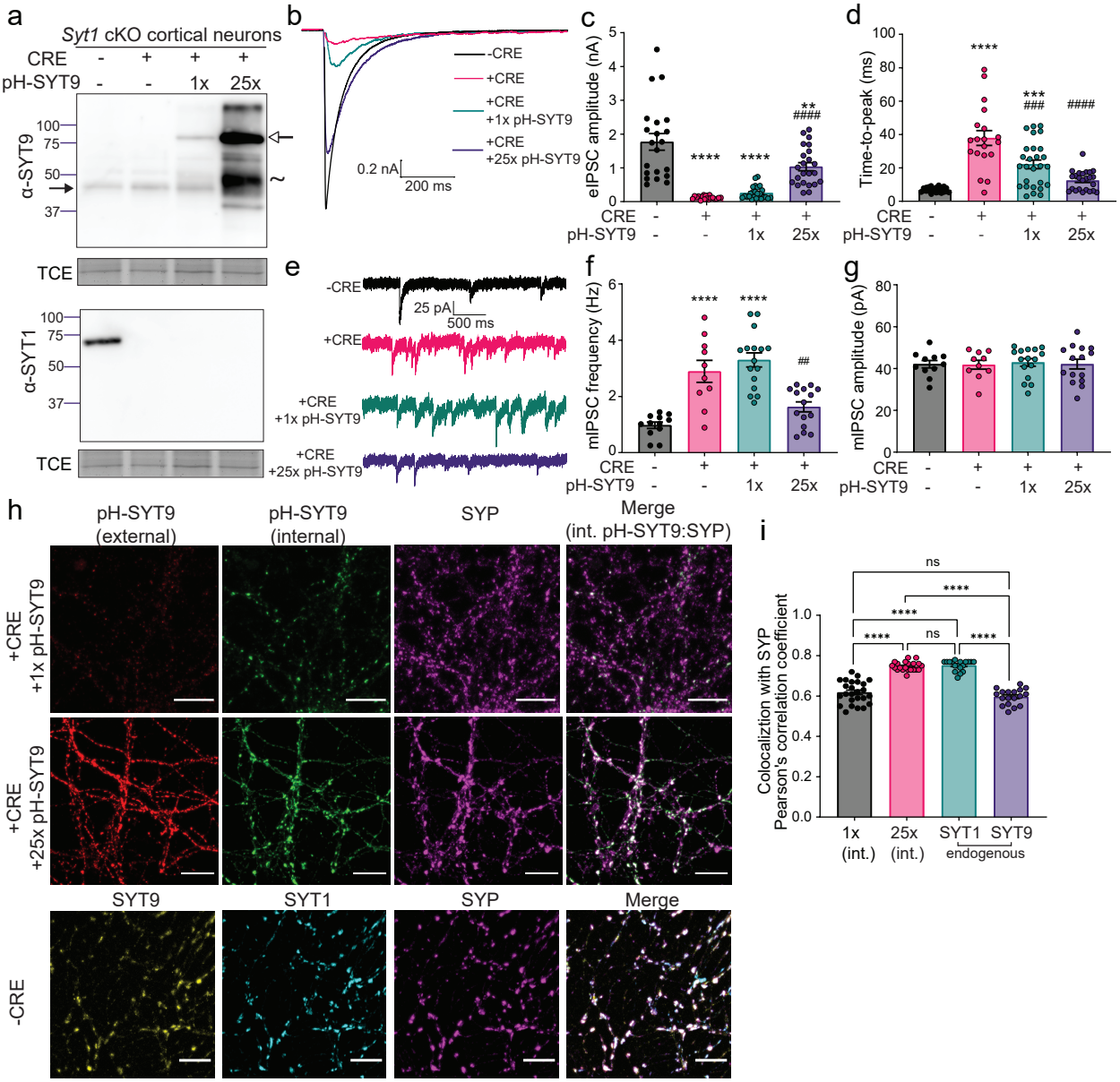

FIGURE 3

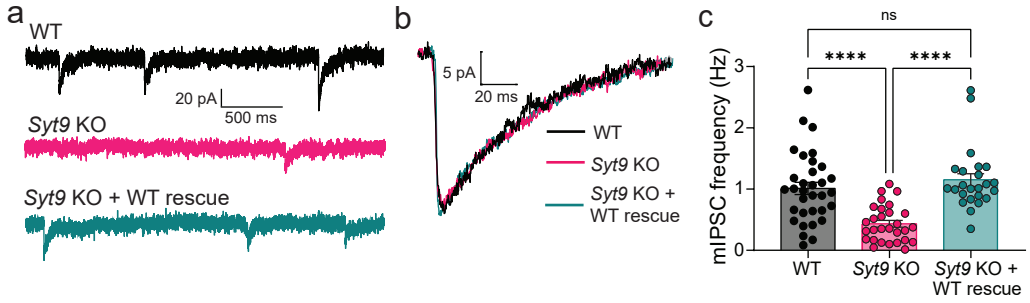

FIGURE 4

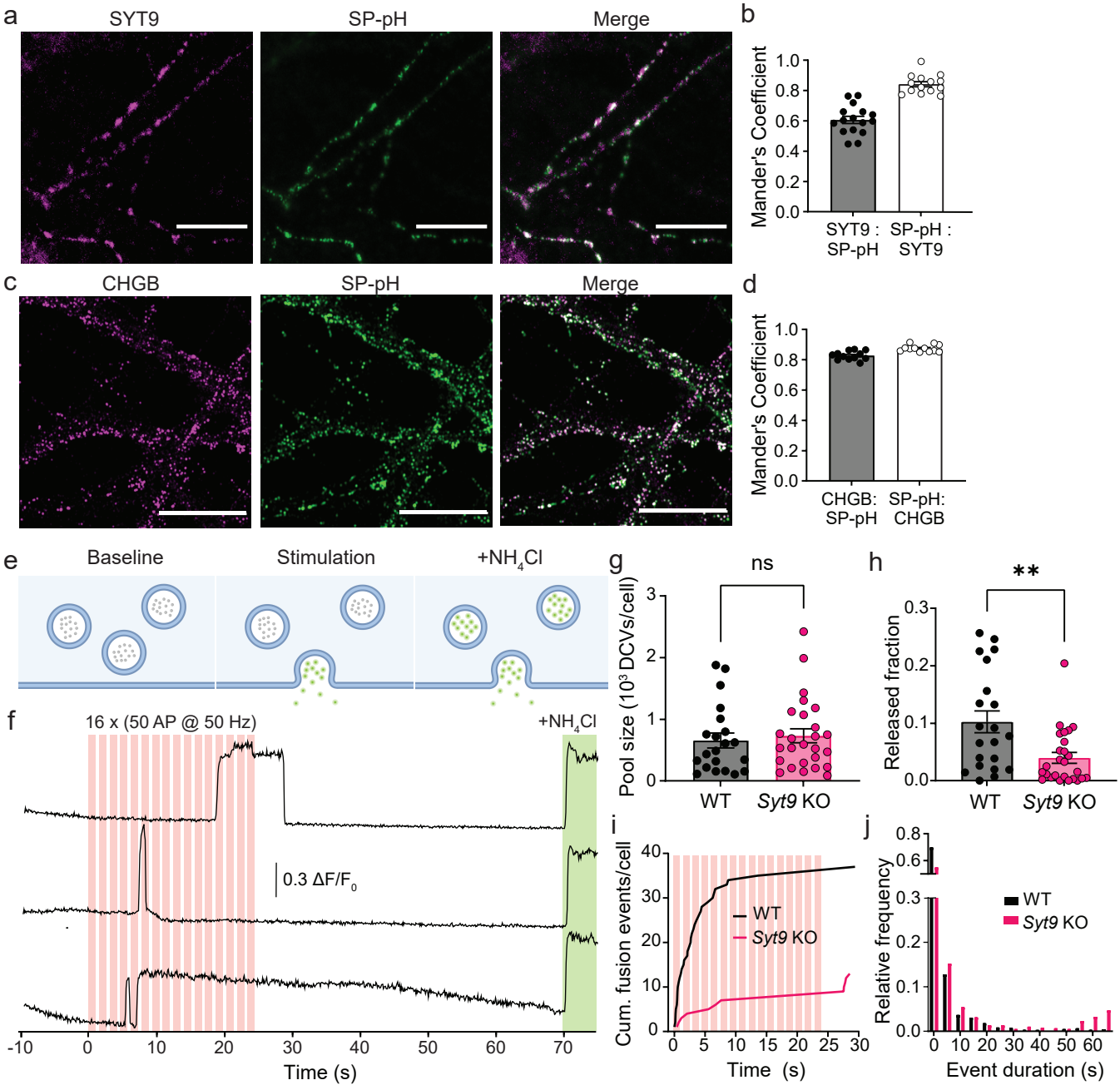

FIGURE 5

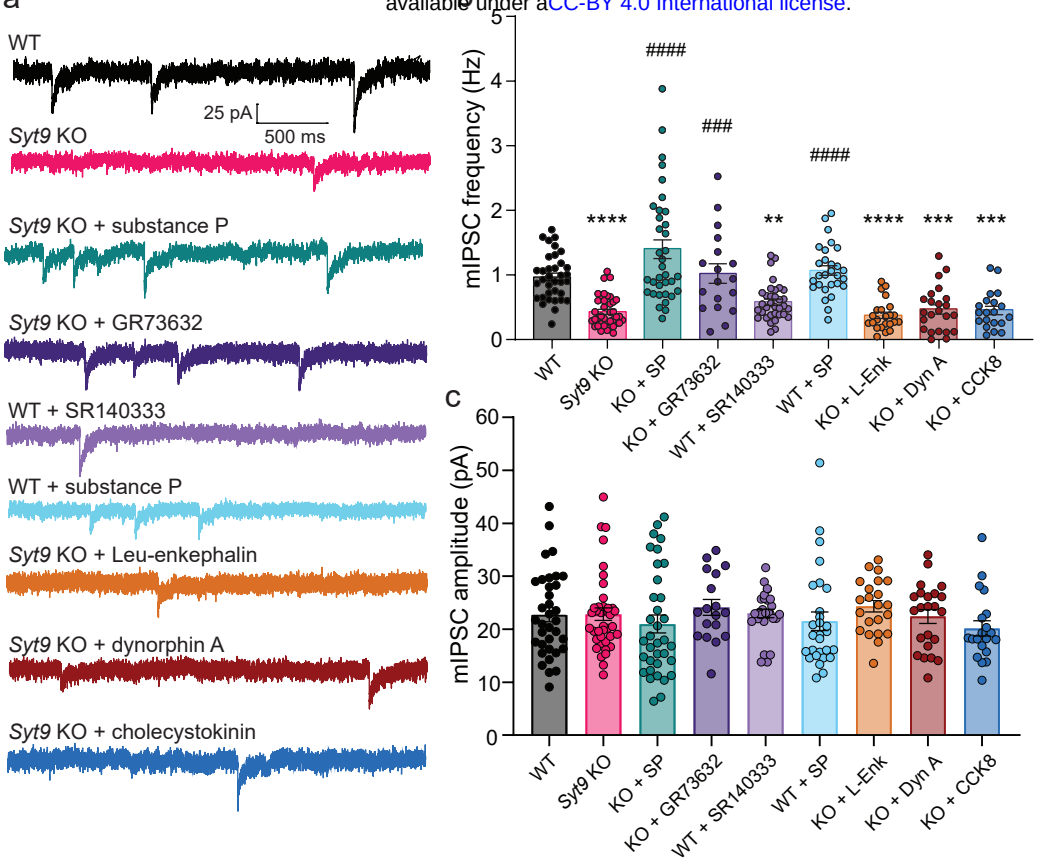

FIGURE 6

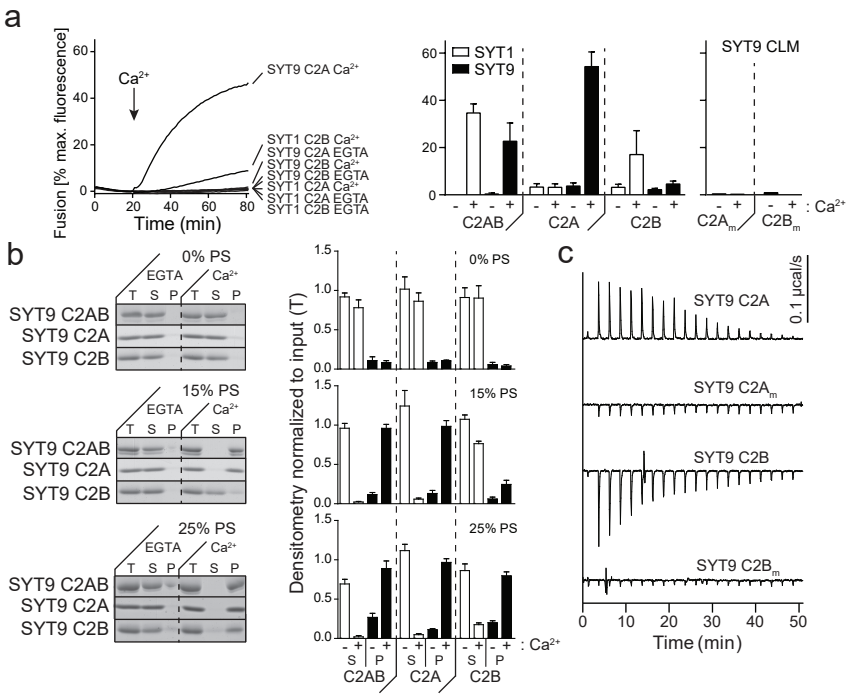

FIGURE 7

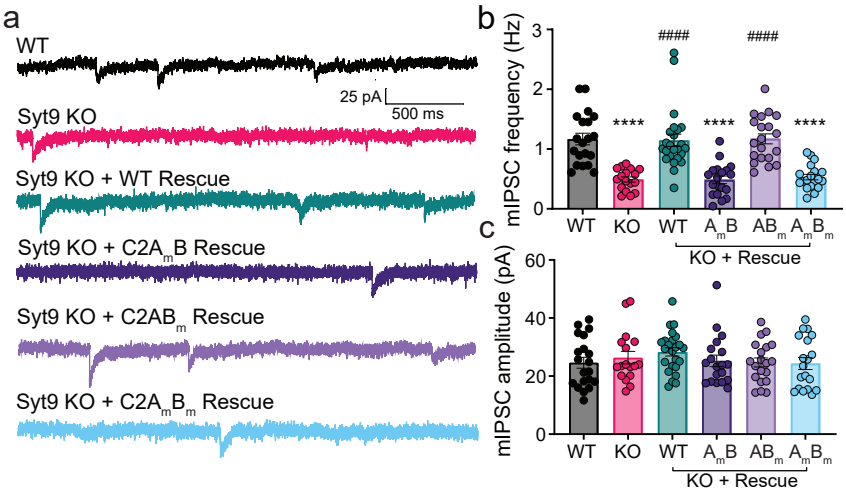

FIGURE 8:

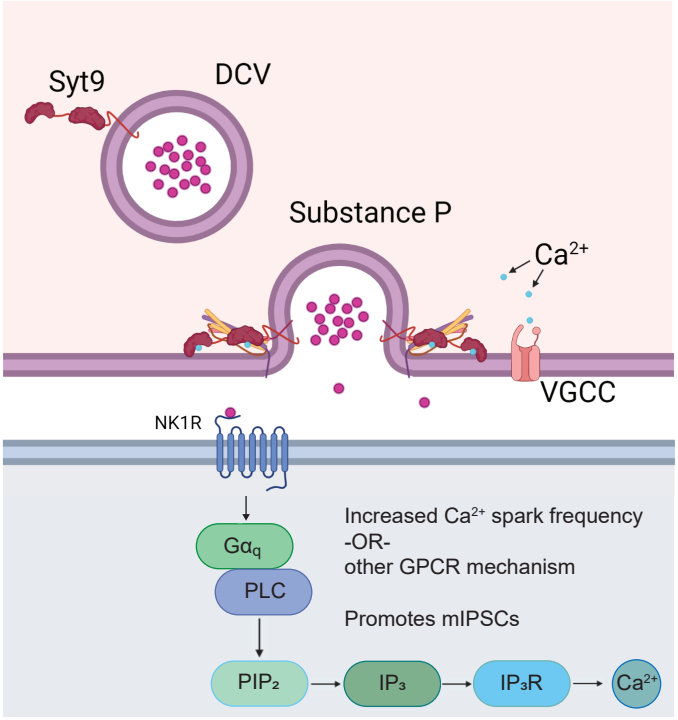

SUPP TABLE 1

Thermodynamic properties of cation binding to isolated C2 domains of SYT9 using ITC

	K_D (mM)	DH (cal/mol)	DS (cal/mol/K)	DG (kcal/mol)
SYT9 C2A	K_{D1}= 53.0 ± 8.6	DH_1= 285 ± 65	DS_1= 20.6 ± 0.49	DG_1= -5.85 ± 0.08
	K_{D2}= 182 ± 39	DH_2= 230 ± 220	DS_2= 18.0 ± 1.1	DG_2= -5.14 ± 0.12
	K_{D3}= 337 ± 80	DH_3= 701 ± 250	DS_3= 18.5 ± 0.50	DG_3= -4.79 ± 0.15
SYT9 C2B	K_{D1}= 42.9 ± 5.5	DH_1= -403 ± 20	DS_1= 18.7 ± 0.30	DG_1= -5.97 ± 0.07
	K_{D2}= 500 ± 95	DH_2= -878 ± 78	DS_2= 12.3 ± 0.58	DG_2= -4.53 ± 0.10

Data presented as mean ± SEM, n=4

SUPP FIG 1

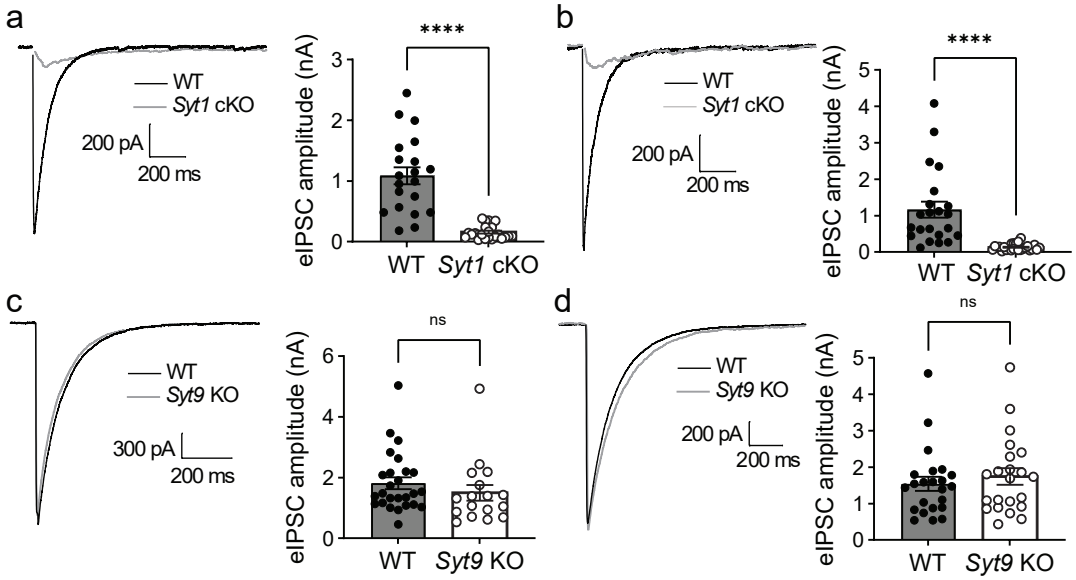

SUPP FIG 2

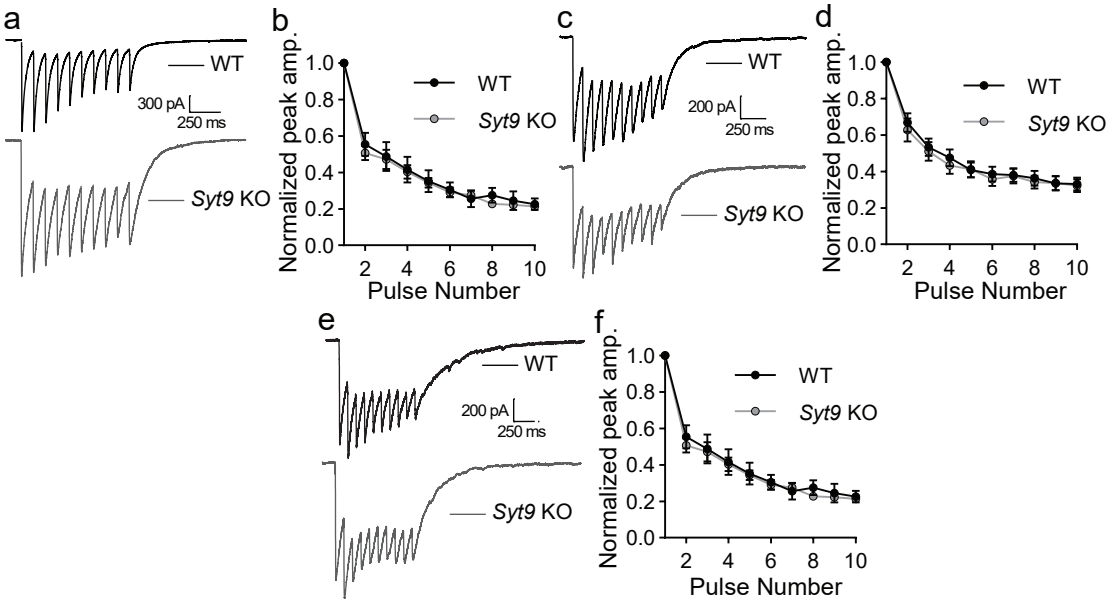

SUPP FIG 3

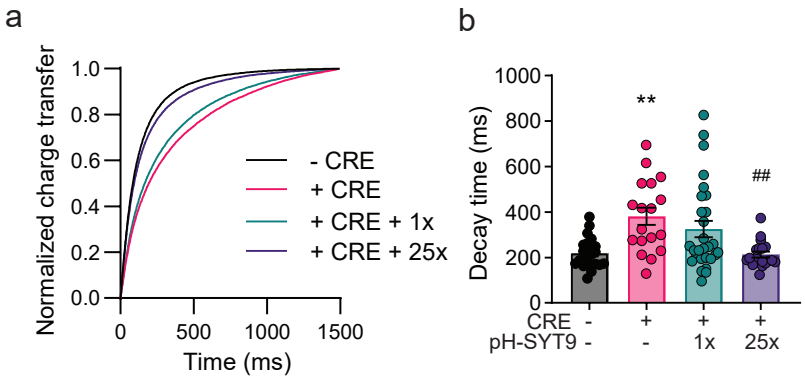

Supp Fig 4

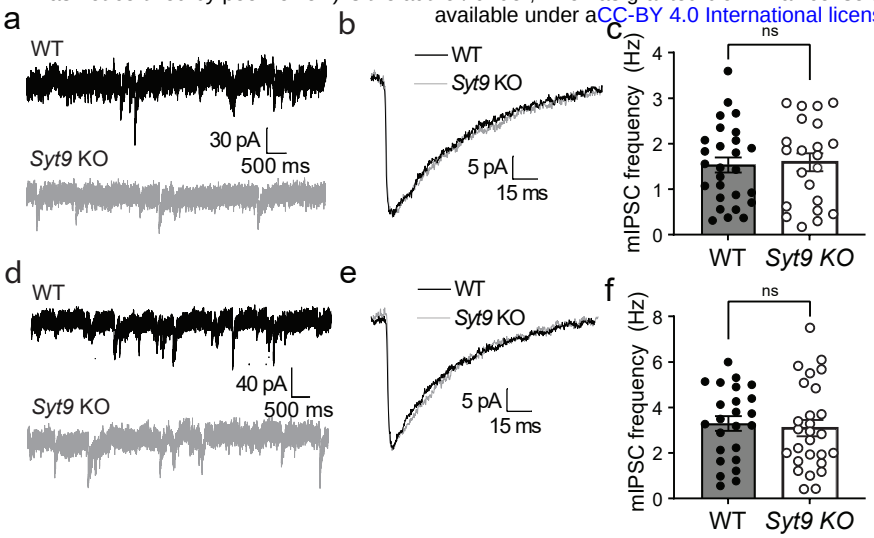

SUPP FIG 5

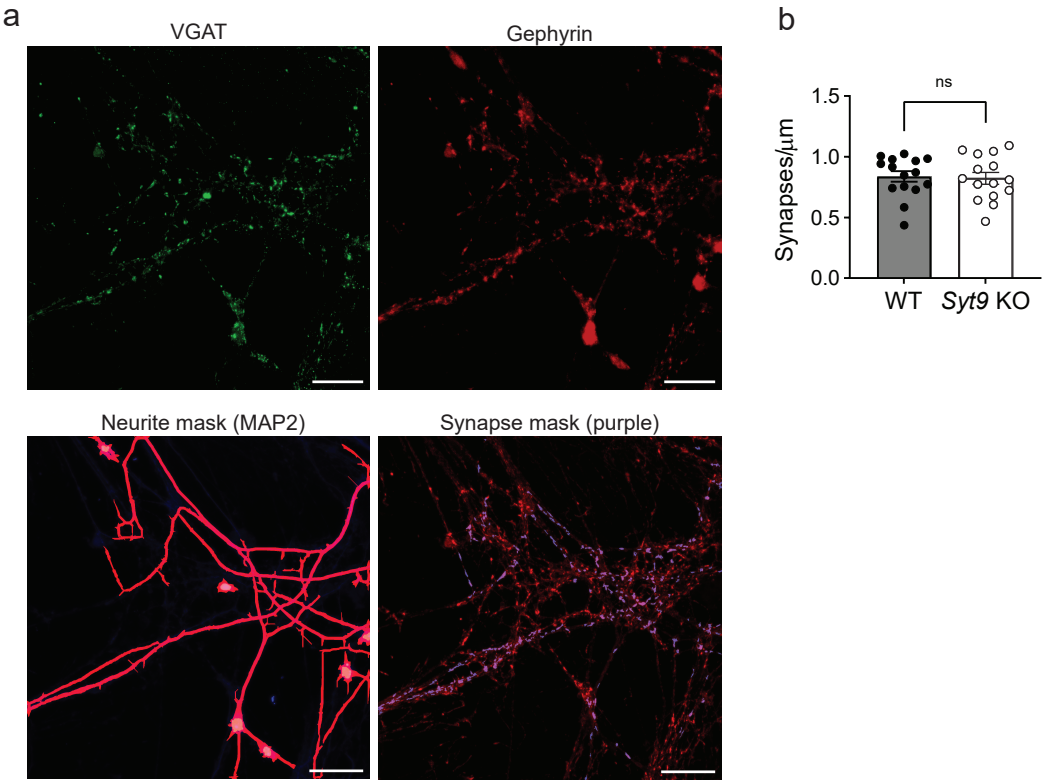

SUPP FIG 6

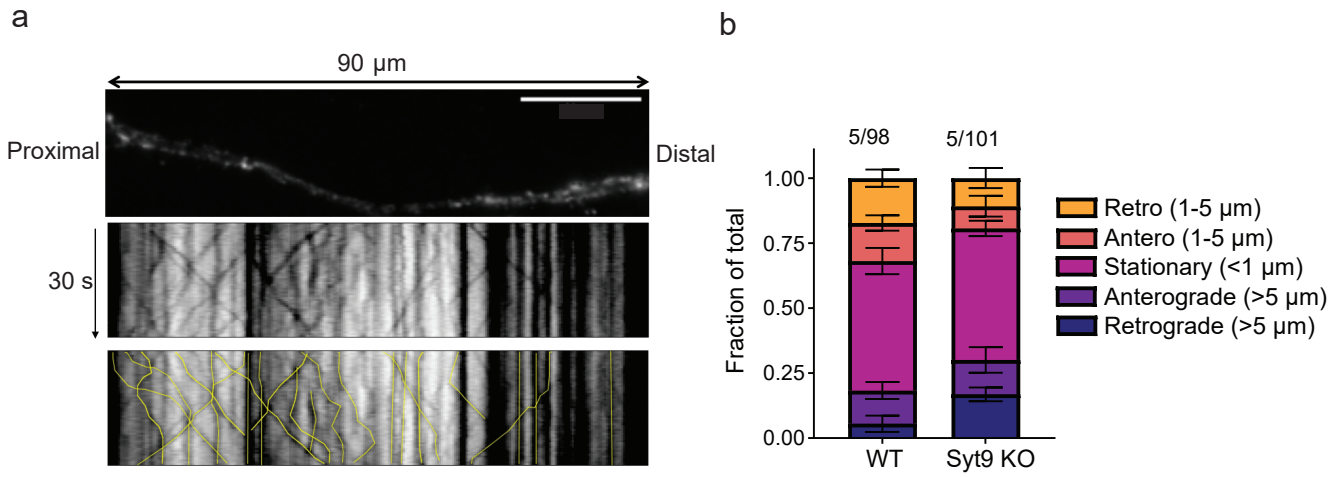

SUPP FIG 7